Theory of charmless inclusive B decays and the extraction of V_{ub}

Björn O. Lange,[1] Matthias Neubert,[2] and Gil Paz[2]

[1]*Center for Theoretical Physics, Massachusetts Institute of Technology, Cambridge, Massachusetts 02139, USA*
[2]*Institute for High-Energy Phenomenology, Newman Laboratory for Elementary-Particle Physics, Cornell University, Ithaca, New York 14853, USA*

(Received 8 June 2005; published 31 October 2005)

We present "state-of-the-art" theoretical expressions for the triple differential $\bar{B} \to X_u l^- \bar{\nu}$ decay rate and for the $\bar{B} \to X_s \gamma$ photon spectrum, which incorporate all known contributions and smoothly interpolate between the "shape-function region" of large hadronic energy and small invariant mass, and the "OPE region" in which all hadronic kinematical variables scale with M_B. The differential rates are given in a form which has no explicit reference to the mass of the b quark, avoiding the associated uncertainties. Dependence on m_b enters indirectly through the properties of the leading shape function, which can be determined by fitting the $\bar{B} \to X_s \gamma$ photon spectrum. This eliminates the dominant theoretical uncertainties from predictions for $\bar{B} \to X_u l^- \bar{\nu}$ decay distributions, allowing for a precise determination of $|V_{ub}|$. In the shape-function region, short-distance and long-distance contributions are factorized at next-to-leading order in renormalization-group improved perturbation theory. Higher-order power corrections include effects from subleading shape functions where they are known. When integrated over sufficiently large portions in phase space, our results reduce to standard OPE expressions up to yet unknown $O(\alpha_s^2)$ terms. Predictions are presented for partial $\bar{B} \to X_u l^- \bar{\nu}$ decay rates with various experimental cuts. An elaborate error analysis is performed that contains all significant theoretical uncertainties, including weak annihilation effects. We suggest that the latter can be eliminated by imposing a cut on high leptonic invariant mass.

DOI: 10.1103/PhysRevD.72.073006 PACS numbers: 12.15.Hh, 13.25.Hw, 12.39.Hg, 12.38.Cy

I. INTRODUCTION

A major effort of the B-physics community is underway to map out the apex of the unitarity triangle, which provides a graphical representation of the effect of CP violation in the quark flavor sector of the standard model. One of the biggest successes of this endeavor was the precise determination of the angle β, which has been measured with high accuracy from the time-dependent CP asymmetry in the $B \to J/\psi K_S$ decay channel [1,2]. The length of the side opposite the angle β is proportional to $|V_{ub}|$. A high-precision determination of this quantity would enable us to test the validity of the standard model and search for possible deviations from its predictions.

Good theoretical knowledge of strong-interaction effects in weak decays of B mesons is crucial for a reliable exploration of the flavor sector of the standard model. In particular, the determination of the Cabibbo-Kobayashi-Maskawa (CKM) matrix elements $|V_{cb}|$ and $|V_{ub}|$ relies on an accurate description of bound-state effects in semileptonic decays. At present, the most precise calculations are available for inclusive semileptonic decays $\bar{B} \to X l^- \bar{\nu}$.

The theoretical tools for the calculation of inclusive B decays are QCD factorization on the one hand [3–11], and local operator product expansions (OPE) on the other [12,13]. Both approaches perform a systematic separation of long-distance hadronic quantities from short-distance perturbative ones, while organizing the calculation in inverse powers of the heavy b-quark mass m_b. The OPE is an appropriate tool for the calculation of total inclusive rates (for example in $\bar{B} \to X_c l^- \bar{\nu}$ decay) or for partial rates integrated over sufficiently large regions in phase space, where all components of the final-state hadronic momentum P_X^μ are large compared to $\Lambda_{\rm QCD}$. QCD factorization, on the other hand, is better suited for the calculation of partial rates and spectra near kinematical boundaries, where typically some components of P_X^μ are large, while the invariant hadronic mass $M_X = \sqrt{P_X^2}$ is small. For example, any $\bar{B} \to X_u l^- \bar{\nu}$ event can be described with three independent kinematical variables, a useful choice of which is [9,14]

$$P_l = M_B - 2E_l, \qquad P_- = E_X + |\vec{P}_X|, \qquad P_+ = E_X - |\vec{P}_X|. \tag{1}$$

Here $P_\pm$ are the light-cone components of the hadronic final-state momentum along the jet direction, E_l is the charged-lepton energy, E_X is the jet energy, and $\vec{P}_X$ is the jet momentum, all measured in the B-meson rest frame. The phase space for these variables is

$$\frac{M_\pi^2}{P_-} \le P_+ \le P_l \le P_- \le M_B, \tag{2}$$

with M_π being the mass of the lightest possible hadronic final state. The product $P_+ P_- = M_X^2$ is the hadronic invariant mass squared. In order to avoid large backgrounds from $b \to c$ transitions, all measurements of $|V_{ub}|$ are in one way or another restricted to the region of phase space where $P_+ P_- < M_D^2$. If the quantity P_- takes values near its maximum at M_B, then P_+ is restricted to a region of

order M_D^2/M_B, which is numerically comparable to $\Lambda_{\rm QCD}$. This means that there are three parametrically different energy scales in the problem: the mass M_B of the initial state, the mass of the final hadronic state $\sim\sqrt{M_B\Lambda_{\rm QCD}}$, and the low-scale $\Lambda_{\rm QCD}$ at which perturbation theory breaks down and hadronic physics must be parameterized in terms of nonperturbative matrix elements. QCD factorization disentangles the effects from these scales, so that the perturbative contributions can be expanded in powers of $\alpha_s(\mu_h)$ with $\mu_h \sim m_b$ (giving rise to ''hard functions'') and $\alpha_s(\mu_i)$ with $\mu_i \sim \sqrt{m_b\Lambda_{\rm QCD}}$ (giving rise to ''jet functions'').

It is important to note that the heavy-quark expansions valid in these two kinematical regions are not identical, because the power-counting rules differ in the two regimes. Also the nature of the nonperturbative inputs is different. In the OPE region, nonperturbative physics is encoded in a few hadronic parameters, and the heavy-quark expansion is the usual Wilsonian expansion in local operators. In the endpoint (or shape-function) region, the presence of multiple scales complicates the power counting, and the interplay between soft and collinear modes gives rise to large nonlocalities. As a result, nonperturbative physics is described by hadronic structure functions called ''shape functions'', and the heavy-quark expansion is an expansion in nonlocal string operators defined on the light-cone. The connections between the two regimes is that *moments* of the shape functions can be expressed in terms of local operators.

The goal of the present work is to develop a formalism that smoothly interpolates between the two kinematical regimes (see [15] for a related discussion, which is however restricted to the tree approximation). This is essential for building an event generator for inclusive $\bar B \to X_u l^- \bar\nu$ and $\bar B \to X_s\gamma$ decays, which can be used to study partial and differential decay rates in different kinematical domains. In the shape-function region, our approach relies on exact QCD factorization theorems, which exist in every order of power counting. They allow us to systematically disentangle short- and long-distance physics and, in the process, resum parametrically large logarithms order by order in perturbation theory. This factorization can be done with high accuracy for the terms of leading power in $1/m_b$, and with somewhat less sophistication for the first-order power corrections. For the second-order power corrections, we only include contributions that do not vanish when integrated over all phase space. This is a safe approximation; the effects of the remaining $1/m_b^2$ terms can to a large extent be absorbed by a redefinition of the subleading shape functions arising at order $1/m_b$.

Our formalism is ''optimized'' for the shape-function region in the sense that sophisticated theoretical technology is applied in this regime. However, when our expressions for the differential decay rates are integrated over sufficiently wide domains, they automatically reduce to the simpler results that can be derived using the OPE approach, up to yet unknown terms of $O(\alpha_s^2)$. The moment relations for the shape functions are crucial in this context. Note that local $1/m_b^2$ corrections in the OPE receive contributions from terms of leading power $(1/m_b^0)$, subleading power $(1/m_b)$, and subsubleading power $(1/m_b^2)$ in the shape-function region, so the transition is highly nontrivial. In implementing the program outlined here, we include all presently known information on the triple differential $\bar B \to X_u l^- \bar\nu$ decay rate and on the differential $\bar B \to X_s\gamma$ decay rate in a single, unified framework. We neglect, for simplicity, hadronic power corrections of order $1/m_b^3$ and higher, which are known to have a negligible effect on the observables considered here. The only possible exception is contributions from ''weak annihilation'', which are estimated as part of our error analysis. We also ignore the existing results on $O(\beta_0\alpha_s^2)$ radiative corrections for some single-differential distributions, because the corresponding corrections are not known for the double or triple differential $\bar B \to X_u l^- \bar\nu$ decay spectra. While these $O(\beta_0\alpha_s^2)$ terms are sometimes found to be large when naive perturbation theory in $\alpha_s(m_b)$ is used, their effects are expected to be small in our scheme, which is based on a complete scale separation using QCD factorization. We see no reason why the $\beta_0\alpha_s^2$ terms should be enhanced compared to other, unknown corrections of $O(\alpha_s^2)$.

A technical complication in realizing the approach described here has to do with the treatment of phase-space factors. The heavy-quark expansion of the hadronic tensor for $\bar B \to X_u l^- \bar\nu$ decay gives rise to expressions that are singular at certain points in phase space. One way to avoid these singularities is to also expand phase-space factors order by order in $1/m_b$ (see, e.g., the treatment in [16]). However, since this expansion depends on the kinematical cuts of any given analysis, it cannot be implemented in a straightforward way in an event generator. An alternative is to reorganize the heavy-quark expansion in such a way that the expansion parameter is related to *hadronic* (as opposed to partonic) kinematical variables, in which case kinematical singularities are always canceled by exact phase-space factors. Following this strategy, we obtain expressions for decay distributions and partial decay rates which are free of explicit reference to partonic quantities such as the b-quark mass. A dependence on m_b enters only implicitly via the first moment of the leading-order shape function $\hat S(\hat\omega)$. The philosophy of our approach is that this function[1] is extracted experimentally from a fit to the $\bar B \to X_s\gamma$ photon spectrum, which has been measured with good precision in the region where $P_+ = M_B - 2E_\gamma \sim \Lambda_{\rm QCD}$. This is analo-

[1]More precisely, we define a new shape function $\hat S(\hat\omega)$ by the combination of leading and subleading shape functions contributing to $\bar B \to X_s\gamma$ decay, and we will use the same function to make predictions for $\bar B \to X_u l^- \bar\nu$ decay distributions.

gous to the extraction of parton distribution functions from deep inelastic scattering. The photon spectrum is experimentally accessible to energies as low as 1.8 GeV, which corresponds to a sampling of the shape function for values of $\hat{\omega}$ up to about 1.7 GeV. Once the shape function has been extracted over this range, we can use it to obtain predictions for arbitrary partial $\bar{B} \to X_u l^- \bar{\nu}$ decay rates with cuts. In doing so, the residual hadronic uncertainties in the extraction of $|V_{ub}|$ only enter at the level of power corrections.

We emphasize that the program outlined above is equivalent to an approach put forward in [4] and later refined in [17–19], in which $|V_{ub}|$ is extracted with the help of shape-function independent relations between weighted integrals over differential decay distributions in $\bar{B} \to X_s\gamma$ and $\bar{B} \to X_u l^- \bar{\nu}$. The experimental error in the results for these weighted integrals corresponds, in our approach, to the error in the prediction of $\bar{B} \to X_u l^- \bar{\nu}$ partial rates resulting from the experimental uncertainty in the extraction of the shape function from the $\bar{B} \to X_s\gamma$ photon spectrum. While the shape-function independent relations are very elegant, it is more convenient for the construction of a generator to have a formulation where the shape function is used as an input. In this way, it is possible to impose arbitrary cuts on kinematical variables without having to recompute the weight functions in each case.

The paper is structured as follows: In Sec. II we collect the relevant formulas for the calculation of the $\bar{B} \to X_s\gamma$ photon spectrum. These expressions can be used to extract the leading nonperturbative structure function from experiment. An analogous presentation for the triple-differential decay rate in $\bar{B} \to X_u l^- \bar{\nu}$ decays is presented in Sec. III. In order to perform a numerical analysis one needs to rely on parametrizations of the shape functions. A collection of several useful functional forms is given in Sec. IV. In Sec. V we present a full error analysis of partial $\bar{B} \to X_u l^- \bar{\nu}$ decay rates for a variety of experimental cuts. We also explore the sensitivity of the results to the b-quark mass and to the functional forms adopted for the shape functions. Sec. VI contains our conclusions.

II. INCLUSIVE RADIATIVE DECAYS

The decay process $\bar{B} \to X_s\gamma$, while more complex in its short-distance physics, is considerably simpler in its kinematics than the semileptonic process $\bar{B} \to X_u l^- \bar{\nu}$. Since the radiated photon is on-shell, the hadronic variables $P_\pm$ that describe the momentum of the X_s system are trivially related to the photon energy E_γ by $P_+ = M_B - 2E_\gamma$ and $P_- = M_B$. In the crudest approximation, namely, at tree level and leading power, the photon-energy spectrum is directly proportional to the leading shape function, $d\Gamma_s/dE_\gamma \propto \hat{S}(P_+)$. In this section we collect all relevant formulas needed to compute the $\bar{B} \to X_s\gamma$ photon spectrum or, equivalently, the invariant hadronic mass distribution. It is implicitly assumed that these spectra are sufficiently "smeared" (e.g., by experimental resolution) to wash out any sharp hadronic structures. In cases where the resolution is such that the K^* resonance peak is observed, it can be accounted for by combining the formulas in this section with the prescription for subtracting the K^* peak proposed in [20].

The differential $\bar{B} \to X_s\gamma$ decay rate can be written as

$$\frac{d\Gamma_s}{dE_\gamma} = \frac{G_F^2\alpha}{2\pi^4} E_\gamma^3 |V_{tb}V_{ts}^*|^2 \overline{m}_b^2(\mu_h) \times [C_{7\gamma}^{\rm eff}(\mu_h)]^2 U(\mu_h, \mu_i) \mathcal{F}_\gamma(P_+), \tag{3}$$

where the structure function $\mathcal{F}_\gamma$ depends on the photon energy via $P_+ = M_B - 2E_\gamma$. The prefactor contains the electromagnetic fine-structure constant α normalized at $q^2 = 0$, two powers of the running b-quark mass (defined in the $\overline{\rm MS}$ scheme) originating from the electromagnetic dipole operator $Q_{7\gamma}$ in the effective weak Hamiltonian, and the square of the corresponding Wilson coefficient $C_{7\gamma}^{\rm eff}$, which is needed at next-to-leading order in renormalization-group improved perturbation theory [21]. Renormalization-group running from the hard scale $\mu_h \sim m_b$ to the intermediate scale $\mu_i \sim \sqrt{m_b\Lambda_{\rm QCD}}$ gives rise to the evolution factor $U(\mu_h, \mu_i)$, whose explicit form is discussed in Appendix A. We keep U and $(C_{7\gamma}^{\rm eff})^2$ outside of the structure function $\mathcal{F}_\gamma$; it is understood that when combining the various terms in (3) all perturbative quantities should be expanded for consistency to the required order in α_s.

A. Leading-power factorization formula

At leading order in $1/m_b$ the structure function $\mathcal{F}_\gamma$ factorizes as [11]

$$\mathcal{F}_\gamma^{(0)}(P_+) = |H_s(\mu_h)|^2 \int_0^{P_+} d\hat{\omega}\; m_b J(m_b(P_+ - \hat{\omega}), \mu_i) \times \hat{S}(\hat{\omega}, \mu_i). \tag{4}$$

At this order a single nonperturbative parton distribution function arises, called the leading shape function [4] and denoted by $\hat{S}(\hat{\omega}, \mu_i)$. Our notation is adopted from [9,16]: hatted shape functions have support for $\hat{\omega} \geq 0$. The function $\hat{S}$ is defined in terms of a nonlocal matrix element in heavy-quark effective theory (HQET). Renormalization-group running between the intermediate scale and a low hadronic scale is avoided when using the shape functions renormalized at the intermediate scale μ_i. Evolution effects below this scale are universal (i.e., process independent) and so can be absorbed into the renormalized shape function. Short-distance contributions from scales above $\mu_h \sim m_b$ are included in the hard function H_s, which in practice is obtained by matching the effective weak Hamiltonian onto a current operator in soft-collinear effective theory (SCET). At next-to-leading order in pertur-

bation theory, the result reads

$$H_s(\mu_h) = 1 + \frac{C_F\alpha_s(\mu_h)}{4\pi}\left(-2\,\ln^2\frac{m_b}{\mu_h} + 7\ln\frac{m_b}{\mu_h} - 6 - \frac{\pi^2}{12}\right) + \varepsilon_{\rm ew} + \frac{C_{8g}^{\rm eff}(\mu_h)}{C_{7\gamma}^{\rm eff}(\mu_h)}\,\frac{C_F\alpha_s(\mu_h)}{4\pi}\left(-\frac{8}{3}\ln\frac{m_b}{\mu_h} + \frac{11}{3} - \frac{2\pi^2}{9} + \frac{2\pi i}{3}\right)$$
$$+ \frac{C_1(\mu_h)}{C_{7\gamma}^{\rm eff}(\mu_h)}\,\frac{C_F\alpha_s(\mu_h)}{4\pi}\left(\frac{104}{27}\ln\frac{m_b}{\mu_h} + g(z) - \frac{V_{ub}V_{us}^*}{V_{tb}V_{ts}^*}[g(0) - g(z)]\right) + \varepsilon_{\rm peng}, \tag{5}$$

where the variable $z = (m_c/m_b)^2$ denotes the ratio of quark masses relevant to charm-loop penguin diagrams, and the "penguin function" $g(z)$ can be approximated by the first few terms of its Taylor expansion,

$$g(z) = -\frac{833}{162} - \frac{20\pi i}{27} + \frac{8\pi^2}{9}z^{3/2} + \frac{2z}{9}[48 - 5\pi^2 - 36\zeta_3 + (30\pi - 2\pi^3)i + (36 - 9\pi^2 + 6\pi i)\ln z$$
$$+ (3 + 6\pi i)\,\ln^2 z + \ln^3 z] + \frac{2z^2}{9}[18 + 2\pi^2 - 2\pi^3 i + (12 - 6\pi^2)\ln z + 6\pi i\,\ln^2 z + \ln^3 z]$$
$$+ \frac{z^3}{27}[-9 - 14\pi^2 + 112\pi i + (182 - 48\pi i)\ln z - 126\,\ln^2 z] + \ldots. \tag{6}$$

The Wilson coefficients C_1 and $C_{8g}^{\rm eff}$ in (5) multiply the current-current operators $Q_1^{u,c}$ and the chromo-magnetic dipole operator Q_{8g} in the effective weak Hamiltonian. The quantities $\varepsilon_{\rm ew} \approx -1.5\%$ and $\varepsilon_{\rm peng} \approx -0.6\%$ account for small electroweak corrections and the effects of penguin contractions of operators other than $Q_1^{u,c}$, respectively. The differential decay rate (3) is formally independent of the matching scales μ_h and μ_i. The μ_h dependence of the evolution factor $U(\mu_h, \mu_i)$ cancels the scale dependence of the product $\overline{m}_b^2(\mu_h)[C_{7\gamma}^{\rm eff}(\mu_h)]^2|H_s(\mu_h)|^2$, while its μ_i dependence compensates the scale dependence of the convolution integral $J(\mu_i) \otimes \hat{S}(\mu_i)$.

Finally let us discuss the jet function J, which appears as the hard-scattering kernel in the convolution integral in (4). It can be written in terms of distributions that act on the shape function $\hat{S}$. At one-loop order, the jet function is given by [8,9]

$$J(p^2, \mu) = \delta(p^2)\left[1 + \frac{C_F\alpha_s(\mu)}{4\pi}(7 - \pi^2)\right] + \frac{C_F\alpha_s(\mu)}{4\pi}\left[\frac{1}{p^2}\left(4\ln\frac{p^2}{\mu^2} - 3\right)\right]_*^{[\mu^2]}, \tag{7}$$

where the star distributions have the following effect on a function f when integrated over a domain Q^2 [22]:

$$\int_{\le 0}^{Q^2} dp^2\left[\frac{1}{p^2}\right]_*^{[\mu^2]} f(p^2) = \int_0^{Q^2} dp^2\,\frac{f(p^2) - f(0)}{p^2} + f(0)\ln\frac{Q^2}{\mu^2},$$
$$\int_{\le 0}^{Q^2} dp^2\left[\frac{1}{p^2}\ln\frac{p^2}{\mu^2}\right]_*^{[\mu^2]} f(p^2) = \int_0^{Q^2} dp^2\,\frac{f(p^2) - f(0)}{p^2}\ln\frac{p^2}{\mu^2} + \frac{f(0)}{2}\ln^2\frac{Q^2}{\mu^2}. \tag{8}$$

B. Kinematical power corrections

There exists a class of power corrections to (4) that do not involve new hadronic quantities. Instead, the power suppression results from the restriction of certain variables (P_+ in the present case) to a region where they are kinematically suppressed (here $P_+ \ll M_B$). The corresponding terms are known in fixed-order perturbation theory, without scale separation and renormalization-group resummation [23,24] (see also [20]). To perform a complete RG analysis of even the first-order terms in $1/m_b$ is beyond the scope of the present work. Since, as we will see later, power corrections only account for small corrections to the decay rates, an approximate treatment will suffice. To motivate it, we note the following two facts [11]: First, while the anomalous dimensions of the relevant subleading SCET and HQET operators are only known for a few cases [25], the leading Sudakov double logarithms are the same as for the terms of leading power, because they have a geometric origin in terms of Wilson lines [26]. The leading Sudakov double logarithms are therefore the same as those resummed into the function U in (3). Secondly, the kinematical power corrections in $\bar{B} \to X_s\gamma$ decay are associated with gluon emission into the hadronic final state X_s. Because of the kinematical restriction to low-mass final states, i.e. $M_X^2 \sim M_B\Lambda_{\rm QCD}$, we associate a coupling $\alpha_s(\bar{\mu})$ with these terms, where typically $\bar{\mu} \sim \mu_i$. Strictly speaking, however, the scale ambiguity associated with the choice of $\bar{\mu}$ could only be resolved by computing the relevant anomalous dimensions.

Within this approximation, the kinematical power corrections to the structure function $\mathcal{F}_\gamma$ can be extracted from [11,20]. We find it convenient to express the result in terms of the variable

$$x = \frac{P_+ - \hat{\omega}}{M_B - P_+}, \tag{9}$$

which in the shape-function region scales like $\Lambda_{\rm QCD}/m_b$. We obtain

$$\mathcal{F}_\gamma{}^{\rm kin}(P_+) = \frac{1}{M_B - P_+}\frac{C_F\alpha_s(\bar{\mu})}{4\pi}\sum_{\substack{i,j=1,7,8\\ i\le j}}\frac{C_i(\mu_h)C_j(\mu_h)}{C_{7\gamma}^{\rm eff}(\mu_h)^2}\int_0^{P_+} d\hat{\omega}\,\hat{S}(\hat{\omega},\mu_i)h_{ij}(x) - \frac{\lambda_2}{9m_c^2}\frac{C_1(\mu_h)}{C_{7\gamma}^{\rm eff}(\mu_h)}\hat{S}(P_+,\mu_i). \tag{10}$$

The coefficient functions $h_{ij}(x)$ are

$$\begin{aligned}
h_{77}(x) &= -3(5+2x) + 2(8+9x+3x^2)\ln\!\left(1+\frac{1}{x}\right),\\
h_{88}(x) &= \frac{2}{9}(1+3x+4x^2+2x^3)\left[2\ln\frac{m_b}{m_s} - \ln\!\left(1+\frac{1}{x}\right)\right]\\
&\quad - \frac{1}{9}(3+9x+16x^2+8x^3),\\
h_{78}(x) &= \frac{2}{3}(5+8x+4x^2) - \frac{8}{3}x(1+x)^2\ln\!\left(1+\frac{1}{x}\right),\\
h_{11}(x) &= \frac{16}{9}\int_0^1 du(1+x-u)\\
&\quad\times\left|\frac{z(1+x)}{u}G\!\left(\frac{u}{z(1+x)}\right)+\frac{1}{2}\right|^2,\\
h_{17}(x) &= -3h_{18}(x)\\
&= -\frac{8}{3}\int_0^1 du\,u\,{\rm Re}\left[\frac{z(1+x)}{u}G\!\left(\frac{u}{z(1+x)}\right)+\frac{1}{2}\right],
\end{aligned} \tag{11}$$

where as before $z = (m_c/m_b)^2$, and

$$G(t) = \begin{cases} -2\arctan^2\sqrt{t/(4-t)}; & t<4,\\ 2(\ln[(\sqrt{t}+\sqrt{t-4})/2] - \frac{i\pi}{2})^2; & t\ge 4. \end{cases} \tag{12}$$

In the shape-function region the expressions for $h_{ij}(x)$ could, if desired, be expanded in a power series in $x = O(\Lambda_{\rm QCD}/m_b)$, and this would generate a series of power-suppressed terms $\mathcal{F}_\gamma{}^{{\rm kin}(n)}(P_+)$ with $n \ge 1$, where the superscript "n" indicates the order in the $1/m_b$ expansion. Note that this expansion would contain single logarithms $\ln x \sim \ln(\Lambda_{\rm QCD}/m_b)$. These are precisely the logarithms that would be resummed in a more proper treatment using effective field-theory methods.

Outside the shape-function region the variable x can take on arbitrarily large positive values, and $\mathcal{F}_\gamma{}^{\rm kin}(P_+)$ is no longer power-suppressed. Note that for $P_+ \to M_B$ (corresponding to $x \to \infty$ and $E_\gamma \to 0$) most functions $h_{ij}(x)$ grow like x^2 or weaker, so that the spectrum tends to a constant. The only (well-known) exception is $h_{88}(x)$, which grows like x^3, giving rise to a $1/E_\gamma$ soft-photon singularity [24]. The main effect of the kinematical power corrections (10) to the photon spectrum is to add a radiative tail extending into the region of small photon energies. These corrections therefore become the more significant the larger the integration domain over E_γ is.

C. Subleading shape-function contributions

At order $1/m_b$ in power counting, different combinations of subleading shape functions enter the $\bar{B} \to X_s\gamma$ and $\bar{B} \to X_u l^-\bar{\nu}$ decay distributions [27–30]. They provide the dominant hadronic power corrections, which must be combined with the kinematical power corrections discussed in the previous section. We include their effects using the results of recent calculations in [16,31,32]. Little is known about the subleading shape functions apart from expressions for their first few moments. In particular, the norms of these functions vanish at tree level, while their first moments are determined by the HQET parameters λ_1 and λ_2, which are defined via the forward B-meson matrix elements of the kinetic-energy and the chromo-magnetic operators, respectively [33].

For the case of $\bar{B} \to X_s\gamma$ decay, subleading shape-function contributions are currently only known for the matrix elements of the dipole operator $Q_{7\gamma}$, and the corresponding hard and jet functions have been computed at tree level. Adopting the notations of [16], the relevant subleading shape functions are $\hat{t}(\hat{\omega})$, $\hat{u}(\hat{\omega})$, and $\hat{v}(\hat{\omega})$. An additional function, called s_0, has been absorbed by a redefinition of the leading shape function, and it is included in our definition of $\hat{S}(\hat{\omega})$. Roughly speaking, $\hat{u}(\hat{\omega})$ is the "light-cone generalization" of the local HQET kinetic-energy operator. The functions $\hat{v}(\hat{\omega})$ and $\hat{t}(\hat{\omega})$ are both generalizations of the local chromo-magnetic HQET operator, but $\hat{t}(\hat{\omega})$ contains also a light-cone chromo-electric operator, which has no equivalent in the local OPE expansion. (Such a contribution arises since there are two external 4-vectors in the SCET expansion, n and v, while there is only v in the HQET expansion.) The contribution of subleading shape functions to the $\bar{B} \to X_s\gamma$ photon spectrum is

$$\begin{aligned}
\mathcal{F}_\gamma{}^{{\rm hadr}(1)}(P_+) = \frac{1}{M_B - P_+}[&-(\bar{\Lambda} - P_+)\hat{S}(P_+) - \hat{t}(P_+)\\
&+ \hat{u}(P_+) - \hat{v}(P_+)].
\end{aligned} \tag{13}$$

Compared to [16], we have replaced $1/m_b$ with $1/(M_B - P_+)$ in the prefactor, which is legitimate at this order. (The form of the shape functions restricts P_+ to be of order

$\Lambda_{\rm QCD}$.) The appearance of the HQET parameter $\bar\Lambda = (M_B - m_b)_{m_b\to\infty}$ is peculiar to the subleading shape-function contributions. This quantity is defined via the first moment of the leading-order shape function [9].

The formula given above can be modified to suit the purpose of extracting the shape function from the photon spectrum better. To this end, we absorb a linear combination of the subleading shape functions into a redefinition of the leading shape function, in such a way that the moment relations for this function remain unchanged to the order we are working. This is accomplished by defining

$$\hat S(\hat\omega) \equiv \hat S(\hat\omega) + \frac{2(\bar\Lambda - \hat\omega)\hat S(\hat\omega) - \hat t(\hat\omega) + \hat u(\hat\omega) - \hat v(\hat\omega)}{m_b}. \tag{14}$$

When using $\hat S$ instead of $\hat S$ in the leading-power formula (4), the subleading shape-function contribution becomes

$$\mathcal{F}_\gamma{}^{\rm hadr(1)}(P_+) = -\frac{3(\bar\Lambda - P_+)}{M_B - P_+}\hat S(P_+). \tag{15}$$

The hatted shape functions used in the present work are related to the original definitions in [16] by

$$\hat S(\hat\omega) = S(\bar\Lambda - \hat\omega) + \frac{s_0(\bar\Lambda - \hat\omega)}{m_b}, \qquad \hat t(\hat\omega) = t(\bar\Lambda - \hat\omega),$$
$$\hat u(\hat\omega) = u(\bar\Lambda - \hat\omega), \qquad \hat v(\hat\omega) = v(\bar\Lambda - \hat\omega), \tag{16}$$

where the unhatted functions have support on the interval between $-\infty$ and $\bar\Lambda$. It is convenient to rewrite $\bar\Lambda - \hat\omega = \omega + \Delta\omega$, where

$$\Delta\omega \equiv \bar\Lambda - (M_B - m_b) = \frac{\lambda_1 + 3\lambda_2}{2m_b} + \ldots \tag{17}$$

accounts for the mismatch between the HQET parameter $\bar\Lambda$ and the difference $(M_B - m_b)$ due to power-suppressed terms in the $1/m_b$ expansion [34]. It follows that the variable $\omega = (M_B - m_b) - \hat\omega$ runs from $-\infty$ to $(M_B - m_b)$. The moment relations for the leading and subleading shape functions derived in [4,16,27] can be summarized as

$$\begin{aligned}
\hat S(\hat\omega) &\equiv S(\omega + \Delta\omega) + \frac{s_0(\omega + \Delta\omega)}{m_b} \\
&= \delta(\omega) - \frac{\lambda_1}{6}\delta''(\omega) + \frac{\lambda_1 + 3\lambda_2}{2m_b}\delta'(\omega) + \ldots, \\
\hat t(\hat\omega) &\equiv t(\omega + \Delta\omega) = \lambda_2\delta'(\omega) + \ldots, \\
\hat u(\hat\omega) &\equiv u(\omega + \Delta\omega) = -\frac{2\lambda_1}{3}\delta'(\omega) + \ldots, \\
\hat v(\hat\omega) &\equiv v(\omega + \Delta\omega) = -\lambda_2\delta'(\omega) + \ldots.
\end{aligned} \tag{18}$$

The function $\hat S$ has the same moment expansion as $\hat S$. The hadronic parameter λ_2 determines the leading contribution to the hyperfine splitting between the masses of B and B^* mesons through $m_{B^*}^2 - m_B^2 = 4\lambda_2 + O(1/m_b)$ [33], from which it follows that $\lambda_2 \approx 0.12\ \text{GeV}^2$. The value of the parameter λ_1 is more uncertain. In much the same way as the b-quark pole mass, it is affected by infrared renormalon ambiguities [35,36]. It is therefore better to eliminate λ_1 in favor of some observable, for which we will choose the width of the leading shape function.

D. Residual hadronic power corrections

At order $1/m_b^2$ a new set of sub-subleading shape functions enter, which so far have not been classified completely in the literature. Since the functional form of even the subleading shape functions is rather uncertain, there is no need to worry too much about the precise form of sub-subleading shape functions. Most of their effects can be absorbed into the subleading functions. An exception, however, are terms that survive when the sub-subleading shape functions are integrated over a wide domain. Whereas the norms of all subleading ($\sim 1/m_b$) shape functions vanish, the norms of the sub-subleading shape functions ($\sim 1/m_b^2$) are in general nonzero and given in terms of the heavy-quark parameters λ_1 and λ_2. (At tree level, the class of functions with nonzero norm has been studied in [15].) Our strategy in the present work will be as follows: We start from the well-known expressions for the (tree-level) second-order power corrections to the $\bar B \to X_s\gamma$ photon spectrum [37] (and similarly for the triple-differential $\bar B \to X_u l^-\bar\nu$ decay distribution [12,13], see Sec. III D). They are of the form λ_i/m_b^2 times one of the singular distributions $\delta(p^2)$, $\delta'(p^2)$, or $\delta''(p^2)$, where $p^2 = (m_b v - q)^2$ is the invariant partonic mass squared of the final-state jet. As mentioned earlier, the power counting in the shape-function region is different from the one used in OPE calculations, and indeed a good portion of the $1/m_b^2$ terms in the OPE is already accounted for by the contributions proportional to the leading and subleading shape functions in (4) and (13). We identify the corresponding terms using the moment relations for the shape functions in (18). In particular, this reproduces all terms at order $1/m_b^2$ in the OPE which contain derivatives of $\delta(p^2)$. We include the remaining terms of the form $(\lambda_i/m_b^2)\delta(p^2)$ by replacing

$$\begin{aligned}
\delta(p^2) = \delta(p_+p_-) &= \frac{1}{p_- - p_+}\int d\omega\,\delta(p_+ + \omega)\delta(\omega) \\
&\to \frac{1}{P_- - P_+}\int d\hat\omega\,\delta(P_+ - \hat\omega)\hat S(\hat\omega) = \frac{\hat S(P_+)}{P_- - P_+}.
\end{aligned} \tag{19}$$

Here $p_\pm$ are the light-cone projections of the partonic momentum p^μ, which are related to the hadronic quantities $P_\pm$ by $P_\pm = p_\pm + (M_B - m_b)$. Similarly, $\hat\omega = (M_B - m_b) - \omega$.

The result of these manipulations is

$$\mathcal{F}_\gamma^{\text{hadr(2)}} = \frac{\lambda_1}{(M_B - P_+)^2}\,\hat{S}(P_+). \tag{20}$$

Together with (4) and (13) this accounts for all known first- and second-order power corrections to the $\bar{B} \to X_s\gamma$ photon spectrum, both in the shape-function region and in the OPE region. The redefinition (14) of the leading shape function from $\hat{S}$ to $\tilde{S}$ leaves the form of the second-order power corrections unaffected.

In Sec. V we study the numerical impact of second-order power corrections on various $\bar{B} \to X_u l^- \bar{\nu}$ partial rates and find their effects to be tiny. It is therefore a safe approximation to neglect hadronic power corrections of order $1/m_b^3$ or higher. The only possible exception to this conclusion relates to the so-called weak annihilation terms in $\bar{B} \to X_u l^- \bar{\nu}$ decay, which will be included in our error analysis.

III. INCLUSIVE SEMILEPTONIC DECAYS

All hadronic physics in $\bar{B} \to X_u l^- \bar{\nu}$ decays is encoded in the hadronic tensor $W^{\mu\nu}$, which is defined via the discontinuity of the forward B-meson matrix element of a correlator of two flavor-changing weak currents $J^\mu = \bar{u}\gamma^\mu(1-\gamma_5)b$. Explicitly,

$$W^{\mu\nu} = \frac{1}{2M_B} \times \frac{1}{\pi}\,\text{Im}\langle \bar{B}(v)|i\int d^4x e^{iq\cdot x}\,\text{T}\{J^{\dagger\mu}(0), J^\nu(x)\}|\bar{B}(v)\rangle, \tag{21}$$

where v is the B-meson velocity and q the momentum carried by the lepton pair. The hadronic tensor can be decomposed into five structure functions W_i, which are the coefficients of the five possible Lorentz structures built out of two independent 4-vectors. Typical choices for these two vectors are q and v, p and v, etc. Here, as above, $p = m_b v - q$ is the momentum of the jet of light particles into which the b quark decays. In principle, all choices are equivalent, and it is solely a matter of convenience which basis one picks.

The triple-differential decay rate can then be expressed in terms of kinematical prefactors and the functions W_i. It is a known fact that the total decay rate is proportional to five powers of the b-quark mass. Further sensitivity to m_b is picked up for partial decay rates by the kinematical cuts. For example, cutting on the leptonic invariant mass $q^2 > q_0^2$ introduces roughly five additional powers, and the resulting partial decay rate is proportional to $(m_b)^a$ with $a \approx 10$ [38,39]. This is the reason why theoretical predictions were typically made for event fractions, so that at least the five powers of m_b in the total rate drop out. For practical purposes, however, this procedure presents no advantage as the value of the total decay rate cannot be measured. Furthermore, the m_b dependence of the total rate is clearly related to the m_b dependence of partial rates, and it is important to take this correlation into account when combining calculations of event fractions with those of the total decay rate. In Sec. V, where we present theoretical predictions, we will thus focus directly on predictions for partial decay rates, not event fractions. Note that information about m_b enters the triple-differential decay rate in two ways, via the hadronic structure functions W_i and through their kinematical prefactors. Whether or not m_b appears explicitly in the prefactors depends on the decomposition of $W^{\mu\nu}$, i.e., on the choice of vectors used to form the five possible Lorentz structures.

A very useful set of 4-vectors turns out to be (v, n), where n is a lightlike vector in the direction of the jet of light particles. In SCET, n denotes the direction of the collinear particles in the jet, which is typically set to be along the z axis. The normalization is chosen such that $v \cdot n = 1$, so that $n^\mu = (1, 0, 0, 1)$ in the rest frame of the B meson. The conjugate direction to n is denoted by $\bar{n}^\mu = (1, 0, 0, -1)$ and marks the direction of the photon in $\bar{B} \to X_s\gamma$ decay, or the direction of the lepton pair in $\bar{B} \to X_u l^- \bar{\nu}$ decay. We then decompose

$$\begin{aligned} W^{\mu\nu} = {} & (n^\mu v^\nu + n^\nu v^\mu - g^{\mu\nu} - i\epsilon^{\mu\nu\alpha\beta} n_\alpha v_\beta)\tilde{W}_1 \\ & - g^{\mu\nu}\tilde{W}_2 + v^\mu v^\nu \tilde{W}_3 + (n^\mu v^\nu + n^\nu v^\mu)\tilde{W}_4 \\ & + n^\mu n^\nu \tilde{W}_5. \end{aligned} \tag{22}$$

The structure functions $\tilde{W}_i$ all have mass dimension -1 in this basis. In terms of the $\tilde{W}_i$ functions the triple-differential decay rate reads

$$\begin{aligned} \frac{d^3\Gamma_u}{dP_+ dP_- dP_l} = {} & \frac{G_F^2|V_{ub}|^2}{16\pi^3}\,U_y(\mu_h, \mu_i)(M_B - P_+) \\ & \times [(P_- - P_l)(M_B - P_- + P_l - P_+)\mathcal{F}_1 \\ & + (M_B - P_-)(P_- - P_+)\mathcal{F}_2 \\ & + (P_- - P_l)(P_l - P_+)\mathcal{F}_3], \end{aligned} \tag{23}$$

where we have collected the relevant combinations of $\tilde{W}_i$ into the three functions

$$\begin{aligned} U_y(\mu_h, \mu_i)\mathcal{F}_1 = \tilde{W}_1, \qquad U_y(\mu_h, \mu_i)\mathcal{F}_2 = \frac{\tilde{W}_2}{2}, \\ U_y(\mu_h, \mu_i)\mathcal{F}_3 = \left(\frac{y}{4}\tilde{W}_3 + \tilde{W}_4 + \frac{1}{y}\tilde{W}_5\right), \end{aligned} \tag{24}$$

and defined a new kinematical variable

$$y = \frac{P_- - P_+}{M_B - P_+}, \tag{25}$$

which can take values $0 \le y \le 1$. The leading evolution factor $U_y(\mu_h, \mu_i)$ has been factored out in (23) for convenience, as we have done earlier in (3). The function $U_y(\mu_h, \mu_i)$ differs from the corresponding function in $\bar{B} \to X_s\gamma$ decay by a y-dependent factor,

$$U_y(\mu_h, \mu_i) = U(\mu_h, \mu_i)\, y^{-2a_\Gamma(\mu_h,\mu_i)}, \tag{26}$$

where the function a_Γ in the exponent is related to the cusp anomalous dimension and is given in Appendix A.

Equation (23) for the triple-differential rate is exact. Note that there is no reference to the b-quark mass at this point. The only dependence on m_b is through the structure functions $\mathcal{F}_i(P_+, y)$ (via hard matching corrections and via the moment constraints on the shape function $\hat{S}$), which are independent of the leptonic variable P_l. The fact that the total decay rate Γ_u is proportional to m_b^5 is not in contradiction with (23). It is instructive to demonstrate how these five powers of m_b are recovered in our approach. At tree level and leading power the functions $\mathcal{F}_2$ and $\mathcal{F}_3$ vanish, while $\mathcal{F}_1 = \hat{S}(P_+)$. Integrating over the full range of P_l and P_- builds up five powers of $(M_B - P_+)$. For the purpose of illustration, let us rename the P_+ variable to $\hat{\omega}$ in the last integration, so that the total decay rate is given as

$$\begin{aligned}\Gamma_u &= \frac{G_F^2|V_{ub}|^2}{192\pi^3}\int_0^{M_B} d\hat{\omega}(M_B - \hat{\omega})^5 \hat{S}(\hat{\omega}) \\ &= \frac{G_F^2|V_{ub}|^2}{192\pi^3}\int_{-m_b}^{M_B - m_b} d\omega(m_b + \omega)^5 S(\omega) \\ &= \frac{G_F^2|V_{ub}|^2}{192\pi^3}(m_b + \langle\omega\rangle)^5\left[1 + O\left(\frac{1}{m_b^2}\right)\right].\end{aligned} \tag{27}$$

At tree level, the first moment of the shape function $S(\omega)$ vanishes. Beyond tree level this is no longer the case, and the average $\langle\omega\rangle$ depends on the size of the integration domain. The above observation motivates the use of the shape-function scheme [9], in which the b-quark mass is defined as $m_b^{\rm SF} = m_b^{\rm pole} + \langle\omega\rangle + O(1/m_b)$. After this is done, (27) recovers the form of the conventional OPE result.

Equation (23) and the above argument tell us that the differential rate is *a priori* rather insensitive to the b-quark mass in the endpoint region, where P_+ (and therefore $\langle\hat{\omega}\rangle$) is a small quantity. Only when the rates are integrated over a sufficiently wide domain, so that shape-function integrals can be approximated using a moment expansion, a dependence on m_b enters indirectly via the first moment of the leading-order shape function. Likewise, a dependence on other HQET parameters such as λ_1 enters via the sensitivity to higher moments.

In the remainder of this section we present the various contributions to the structure functions $\mathcal{F}_i$, following the same line of presentation as we did in the case of $\bar{B} \to X_s\gamma$ decay in Sec. II. As before, while the resulting expressions are optimized for the shape-function region, they can be used over the entire phase space and give the correct result for the total decay rate up to corrections of $O(\alpha_s^2)$. In the shape-function region, where P_+ is a small quantity, one may organize each $\mathcal{F}_i$ as a series in inverse powers of $1/(M_B - P_+)$. No assumption about the variable y is made, which is treated as an $O(1)$ quantity.[2] A preview of the results of our calculation is depicted in Fig. 1, which shows an illustration of our prediction for the distribution of events in the plane (P_+, P_-).

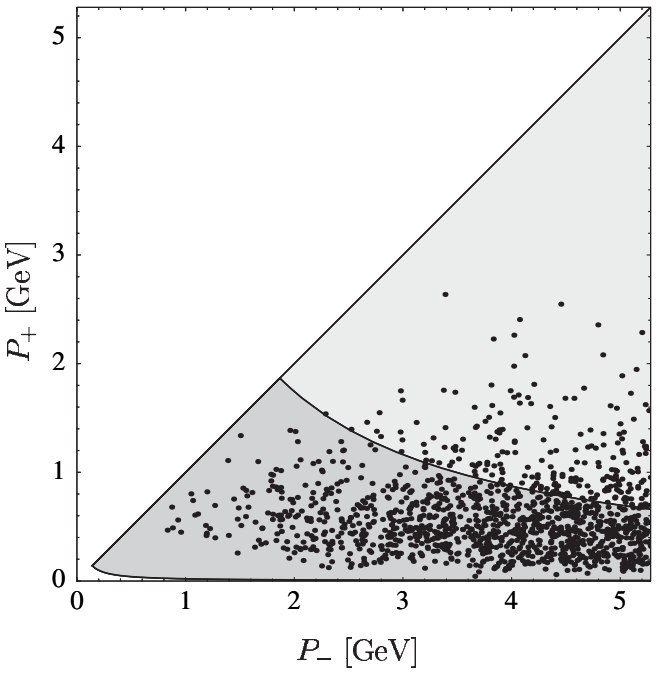

FIG. 1. The hadronic phase space in P_+ and P_-. The light gray region contains background from $\bar{B} \to X_c l^- \bar{\nu}$ decays, while the dark gray region is only populated by $\bar{B} \to X_u l^- \bar{\nu}$ events. The line separating the two regions is the contour where $M_X^2 = P_+P_- = M_D^2$. Each point represents a $\bar{B} \to X_u l^- \bar{\nu}$ event in a Monte-Carlo simulation using the results of this paper. While the shape-function region of large P_- and small P_+ is highly populated, there is not a single event with P_+ larger than 3 GeV out of the 1300 events generated.

A. Leading-power factorization formula

The leading-power expressions for the hadronic structure functions W_i have been calculated in [9] at one-loop order in renormalization-group improved perturbation theory. At this level $\mathcal{F}_2$ does not obtain a contribution, whereas $\mathcal{F}_1$ and $\mathcal{F}_3$ do. Symbolically, they take the factorized form $H_{ui}\, J \otimes \hat{S}$, consisting of hard functions H_{ui} and the convolution of the jet function J with the leading shape function $\hat{S}$. More precisely,

$$\begin{aligned}\mathcal{F}_i^{(0)}(P_+, y) = H_{ui}(y, \mu_h)\int_0^{P_+} d\hat{\omega}\; y m_b J(y m_b(P_+ - \hat{\omega}), \mu_i) \\ \times \hat{S}(\hat{\omega}, \mu_i),\end{aligned} \tag{28}$$

where the hard functions are given by

[2] In the shape-function region, where $P_+ \ll P_-$, we have $y \approx p_-/m_b$, which is the variable used in the leading-power analysis in [9].

$$H_{u1}(y,\mu_h) = 1 + \frac{C_F\alpha_s(\mu_h)}{4\pi}\bigg[-4\ln^2\frac{ym_b}{\mu_h} + 10\ln\frac{ym_b}{\mu_h} - 4\ln y - \frac{2\ln y}{1-y} - 4L_2(1-y) - \frac{\pi^2}{6} - 12\bigg],$$
$$H_{u3}(y,\mu_h) = \frac{C_F\alpha_s(\mu_h)}{4\pi}\,\frac{2\ln y}{1-y}, \qquad (29)$$

and $H_{u2} = 0$. As before, the differential decay rate is independent of the matching scales $\mu_h \sim m_b$ and $\mu_i \sim \sqrt{m_b\Lambda_{\rm QCD}}$. The jet function J has already been given in (7). Note that the b-quark mass appears only as the argument of logarithms, where it plays the role of setting the renormalization scale.

B. Kinematical power corrections

As in the case of $\bar B \to X_s\gamma$ decay, there is a class of power corrections to the $\bar B \to X_u l^-\bar\nu$ decay distributions which are small only because of the restriction to certain regions in phase space, but which are not associated with new hadronic parameters. In the present case, these terms can be extracted from the one-loop expressions derived in [22]. They are then convoluted with the leading shape function. As previously, the scale separation that can be achieved for these power-suppressed terms is only approximate, and we thus assign a coupling $\alpha_s(\bar\mu)$ with them, where the scale $\bar\mu$ is expected to be of order $\mu_i \sim \sqrt{m_b\Lambda_{\rm QCD}}$.

The resulting expressions for the structure functions can be written in a compact form in terms of the variables x and y defined in (9) and (25). We find

$$\mathcal{F}_1^{\rm kin}(P_+,y) = \frac{1}{M_B-P_+}\,\frac{C_F\alpha_s(\bar\mu)}{4\pi}\int_0^{P_+} d\hat\omega\,\hat S(\hat\omega,\mu_i) \times\bigg[\frac{f_1(x,y)}{(1+x)^2y(x+y)} - \frac{2g_1(x,y)}{x(1+x)^2y^2(x+y)} \times\ln\Big(1+\frac{y}{x}\Big) - \frac{4}{x}\ln\Big(y+\frac{y}{x}\Big)\bigg],$$
$$\mathcal{F}_2^{\rm kin}(P_+,y) = \frac{1}{M_B-P_+}\,\frac{C_F\alpha_s(\bar\mu)}{4\pi}\int_0^{P_+} d\hat\omega\,\hat S(\hat\omega,\mu_i) \times\bigg[\frac{f_2(x,y)}{(1+x)^2y^2(x+y)} - \frac{2xg_2(x,y)}{(1+x)^2y^3(x+y)} \times\ln\Big(1+\frac{y}{x}\Big)\bigg],$$
$$\mathcal{F}_3^{\rm kin}(P_+,y) = \frac{1}{M_B-P_+}\,\frac{C_F\alpha_s(\bar\mu)}{4\pi}\int_0^{P_+} d\hat\omega\,\hat S(\hat\omega,\mu_i) \times\bigg[\frac{f_3(x,y)}{(1+x)^2y^3(x+y)} + \frac{2g_3(x,y)}{(1+x)^2y^4(x+y)} \times\ln\Big(1+\frac{y}{x}\Big)\bigg], \qquad (30)$$

where the functions f_i, g_i are given by

$$\begin{aligned}
f_1(x,y) &= -9y + 10y^2 + x(-16 + 12y + 6y^2) + x^2(13y - 12),\\
g_1(x,y) &= -2y^3 - 2xy^2(4+y) - x^2y(12 + 4y + y^2) - 4x^3(y+2) + 3x^4(y-2),\\
f_2(x,y) &= y^2 + xy(8 + 4y + y^2) + 3x^2y(10 + y) + x^3(12 + 19y) + 10x^4,\\
g_2(x,y) &= 2y^2 + 4xy(1+2y) + x^2y(18 + 5y) + 6x^3(1+2y) + 5x^4,\\
f_3(x,y) &= 2y^3(2y - 11) + xy^2(-94 + 29y + 2y^2) + 2x^2y(-72 + 18y + 13y^2) + x^3(-72 - 42y + 70y^2 - 3y^3) - 10x^4(6 - 6y + y^2),\\
g_3(x,y) &= 4y^4 - 6x(y-5)y^3 - 4x^2y^2(-20 + 6y + y^2) + x^3y(90 - 10y - 28y^2 + y^3) + x^4(36 + 36y - 50y^2 + 4y^3) + 5x^5(6 - 6y + y^2).
\end{aligned} \qquad (31)$$

The above formulas are the exact $O(\alpha_s)$ corrections to the leading-power expression. This means that, when integrated over the entire phase space, they will give rise to the correct result for the total rate up to that order. In the shape-function region (where $P_+ \ll P_-$) the integrands in (30) can be expanded in powers of $1/m_b$ by counting $y = O(1)$ and $x = O(1/m_b)$. Note that this organizes the $1/m_b$ expansion as an expansion in powers of the hadronic variable $1/(M_B - P_+)$. The leading terms read

$$\mathcal{F}_1^{\rm kin(1)}(P_+,y) = \frac{1}{M_B-P_+}\,\frac{C_F\alpha_s(\bar\mu)}{4\pi}\int_0^{P_+} d\hat\omega\,\hat S(\hat\omega,\mu_i) \times\bigg[6 - \frac{5}{y} + \Big(\frac{12}{y} - 4\Big)\ln\frac{y}{x}\bigg],$$
$$\mathcal{F}_2^{\rm kin(1)}(P_+,y) = \frac{1}{M_B-P_+}\,\frac{C_F\alpha_s(\bar\mu)}{4\pi}\int_0^{P_+} d\hat\omega\,\hat S(\hat\omega,\mu_i) \times\bigg[\frac{1}{y}\bigg],$$
$$\mathcal{F}_3^{\rm kin(1)}(P_+,y) = \frac{1}{M_B-P_+}\,\frac{C_F\alpha_s(\bar\mu)}{4\pi}\int_0^{P_+} d\hat\omega\,\hat S(\hat\omega,\mu_i) \times\bigg[4 - \frac{22}{y} + \frac{8}{y}\ln\frac{y}{x}\bigg]. \qquad (32)$$

Further accuracy can be achieved by adding the next-order corrections, for which we obtain

$$\mathcal{F}_1^{\rm kin(2)}(P_+,y)=\frac{1}{(M_B-P_+)^2}\frac{C_F\alpha_s(\bar\mu)}{4\pi}\int_0^{P_+}d\hat\omega(P_+-\hat\omega)\hat S(\hat\omega,\mu_i)\bigg[-12+\frac{16}{y}+\frac{3}{y^2}+\Big(\frac{12}{y^2}-\frac{20}{y}+6\Big)\ln\frac{y}{x}\bigg],$$
$$\mathcal{F}_2^{\rm kin(2)}(P_+,y)=\frac{1}{(M_B-P_+)^2}\frac{C_F\alpha_s(\bar\mu)}{4\pi}\int_0^{P_+}d\hat\omega(P_+-\hat\omega)\hat S(\hat\omega,\mu_i)\bigg[1+\frac{2}{y}+\frac{7}{y^2}-\frac{4}{y^2}\ln\frac{y}{x}\bigg], \tag{33}$$
$$\mathcal{F}_3^{\rm kin(2)}(P_+,y)=\frac{1}{(M_B-P_+)^2}\frac{C_F\alpha_s(\bar\mu)}{4\pi}\int_0^{P_+}d\hat\omega(P_+-\hat\omega)\hat S(\hat\omega,\mu_i)\bigg[-6+\frac{69}{y}-\frac{64}{y^2}+\Big(\frac{52}{y^2}-\frac{28}{y}\Big)\ln\frac{y}{x}\bigg].$$

In the various phase-space regions of interest to the determination of $|V_{ub}|$, the above terms (32) and (33) approximate the full result (30) very well (see Sec. V below).

Let us comment here on a technical point already mentioned in the Introduction. When combined with the phase-space factors in (23), the exact expressions for $\mathcal{F}_i^{\rm kin}$ in (30) are regular in the limit $P_-\to P_+$, corresponding to $y\to 0$. However, this feature is not automatically ensured when the structure functions, but not the phase-space factors, are expanded about the heavy-quark limit. With our choice of the variables x and y, we encounter terms as singular as $1/y^n$ at n-th order in the expansion, as is obvious from the explicit expressions above. Phase space scales like y^2 in the limit $y\to 0$ (note that $P_l\to P_+$ as $P_-\to P_+$ because of (2)), so that the results (32) and (33) can be applied without encountering any kinematical singularities. In order to achieve this, it was crucial to define the variable y in the way we did in (25). We emphasize this point because straightforward application of the technology of SCET and HQET developed in [16,31,32] would give an expansion of the structure functions $\mathcal{F}_i$ in powers of $1/p_-$, whereas phase space is proportional to $4\vec p^{\,2}=(p_--p_+)^2\propto y^2$. In the kinematical region where $p_+<0$, which is allowed due to off-shell effects in the B meson, this leads to singularities as $p_-\to 0$. In order to avoid these singularities, we have reorganized the SCET expansion as an expansion in $1/(p_--p_+)$ instead of $1/p_-$, where $|p_+|\ll p_-$ in the shape-function region.

C. Subleading shape-function contributions

The contributions from subleading shape functions to arbitrary $\bar B\to X_u l^-\bar\nu$ decay distributions have been derived (at tree level) in [16,31,32]. The results involve the same set of subleading shape functions as previously discussed in Sec. II C. Again, the structure function $\mathcal{F}_2$ does not obtain a contribution, while

$$\mathcal{F}_1^{\rm hadr(1)}(P_+,y)=\frac{1}{M_B-P_+}\bigg[(\bar\Lambda-P_+)\hat S(P_+)+\hat t(P_+)+\frac{\hat u(P_+)-\hat v(P_+)}{y}\bigg],$$
$$\mathcal{F}_3^{\rm hadr(1)}(P_+,y)=\frac{1}{M_B-P_+}\frac{2}{y}\bigg[-(\bar\Lambda-P_+)\hat S(P_+)-2\hat t(P_+)+\frac{\hat t(P_+)+\hat v(P_+)}{y}\bigg]. \tag{34}$$

At this point we recall the discussion of Sec. II C, where we have argued that the $\bar B\to X_s\gamma$ photon spectrum should be used to fit the function $\hat S$ of (14), which is defined to be a linear combination of the leading shape function $\hat S$ and the subleading shape functions $\hat t$, $\hat u$, $\hat v$. When the above results are rewritten in terms of the new function $\hat S$ nothing changes in the expressions for $\mathcal{F}_i^{(0)}$ except for the simple replacement $\hat S\to\hat S$, which we from now on assume. At the level of subleading shape functions $\mathcal{F}_2^{\rm hadr(1)}=0$ and $\mathcal{F}_3^{\rm hadr(1)}$ remain unchanged, while

$$\mathcal{F}_1^{\rm hadr(1)}(P_+,y)=\frac{1}{M_B-P_+}\bigg[-(\bar\Lambda-P_+)\hat S(P_+)+2\hat t(P_+)+[\hat u(P_+)-\hat v(P_+)]\Big(\frac{1}{y}-1\Big)\bigg]. \tag{35}$$

It follows that there reside some linear combinations of subleading shape functions in the triple-differential decay rate that cannot be extracted from information on the photon spectrum in $\bar B\to X_s\gamma$ decays. In the end, this dependence gives rise to a theoretical uncertainty.

D. Residual hadronic power corrections

In analogy with our treatment for the case of $\bar B\to X_s\gamma$ decay, we start from the expressions for the $1/m_b^2$ corrections to the triple-differential $\bar B\to X_u l^-\bar\nu$ decay rate obtained by applying the OPE to the hadronic tensor [12,13]. Converting these results into the (v,n) basis and changing variables from $v\cdot q$ and q^2 to $p_+=n\cdot p$ and $p_-=\bar n\cdot p$, we find

$$\tilde{W}_1^{(2)} = \delta(p_+)\left(1 + \frac{2\lambda_1 - 3\lambda_2}{3p_-^2}\right) + \delta'(p_+)\left(\frac{2\lambda_1 - 3\lambda_2}{3p_-} - \frac{5\lambda_1 + 15\lambda_2}{6m_b}\right) - \delta''(p_+)\frac{\lambda_1}{6},$$
$$\tilde{W}_2^{(2)} = \delta(p_+)\left(-\frac{4\lambda_1 - 6\lambda_2}{3p_-^2}\right),$$
$$\frac{y}{4}\tilde{W}_3^{(2)} + \tilde{W}_4^{(2)} + \frac{1}{y}\tilde{W}_5^{(2)} = \frac{\delta(p_+)}{p_-}\left(\frac{2\lambda_1 + 12\lambda_2}{3p_-} - \frac{4\lambda_1 + 9\lambda_2}{3m_b}\right) + \frac{\delta'(p_+)}{p_-}\left(\frac{2\lambda_1}{3} + 4\lambda_2\right). \tag{36}$$

The desired $1/(M_B - P_+)^2$ corrections to the structure functions $\mathcal{F}_i$ can then be extracted by expanding the leading and subleading contributions $\mathcal{F}_i^{(0)}$ and $\mathcal{F}_i^{\mathrm{hadr}(1)}$ in terms of their moments in (18), and by subtracting the results from (36). Following the same procedure as in Section II D to express the remaining power corrections in terms of the leading shape function, we obtain

$$\mathcal{F}_1^{\mathrm{hadr}(2)}(P_+, y) = \frac{1}{(M_B - P_+)^2}\left(\frac{4\lambda_1 - 6\lambda_2}{3y^2} - \frac{\lambda_1 + 3\lambda_2}{3}\right) \times \hat{S}(P_+),$$
$$\mathcal{F}_2^{\mathrm{hadr}(2)}(P_+, y) = \frac{1}{(M_B - P_+)^2}\left(\frac{-2\lambda_1 + 3\lambda_2}{3y^2}\right)\hat{S}(P_+),$$
$$\mathcal{F}_3^{\mathrm{hadr}(2)}(P_+, y) = \frac{1}{(M_B - P_+)^2}\left(\frac{4\lambda_1 + 24\lambda_2}{3y^2} - \frac{4\lambda_1 + 9\lambda_2}{3y}\right) \times \hat{S}(P_+). \tag{37}$$

These expressions remain unchanged when the shape function $\hat{S}$ is used instead of $\hat{S}$.

E. Weak annihilation contributions

In the OPE calculation several contributions appear at third order in the power expansion: $1/m_b$ corrections to the kinetic and chromo-magnetic operators, the Darwin and spin-orbit terms, and weak annihilation contributions. The Darwin and spin-orbit terms correspond to the forward B-meson matrix elements of (light) flavor-singlet operators [40]. The corresponding HQET parameters ρ_D^3 and ρ_{LS}^3 can in principle be extracted from moments of inclusive $\bar{B} \to X_c l^- \bar{\nu}$ decay spectra. They are insensitive to the flavor of the spectator quark inside the B meson. The weak annihilation contribution, on the other hand, results from four-quark operators with flavor nonsinglet structure. Graphically, this contribution corresponds to a process in which the b and $\bar{u}$ quark annihilate into a W^-. Weak annihilation terms come with a phase-space enhancement factor of $16\pi^2$ and so are potentially more important than other power corrections of order $1/m_b^3$. Because of the flavor dependence, these contributions can effect neutral and charged B mesons differently [41]. One choice of basis for the corresponding four-quark operators is [42]

$$\langle \bar{B}|\bar{b}_L \gamma_\mu u_L \bar{u}_L \gamma^\mu b_L|\bar{B}\rangle = \frac{f_B^2 M_B^2}{4} B_1,$$
$$\langle \bar{B}|\bar{b}_R u_L \bar{u}_L b_R|\bar{B}\rangle = \frac{f_B^2 M_B^2}{4} B_2, \tag{38}$$

where f_B is the B-meson decay constant, and B_i are hadronic parameters. In the vacuum saturation approximation they are given by $B_1 = B_2 = 1$ for charged B mesons and $B_1 = B_2 = 0$ for neutral ones. The total semileptonic rate is proportional to the difference $(B_2 - B_1)$, which implies that the weak annihilation contribution would vanish in this approximation. Currently, only rough estimates are available for the magnitude of the deviation of this difference from zero. The resulting effect on the total branching ratio is [43]

$$\delta B(\bar{B} \to X_u l^- \bar{\nu}) \approx 3.9\left(\frac{f_B}{0.2\ \mathrm{GeV}}\right)^2\left(\frac{B_2 - B_1}{0.1}\right)|V_{ub}|^2. \tag{39}$$

Again, we expect this effect to be different for charged and neutral B mesons. The most important feature of weak annihilation is that it is formally concentrated at the kinematical point where all the momentum of the heavy quark is transferred to the lepton pair [41]. At the parton level this implies that the corresponding contribution is proportional to $\delta(q^2 - m_b^2)$. It is therefore included in every cut that includes the q^2 endpoint, and its effect is independent of the specific form of the cut.

We suggest two different strategies to control this effect. The first is to include it in the error estimate as a constant contribution proportional to the total rate. A recent study [44] puts a limit on this effect of $\pm 1.8\%$ on the total rate (at 68% confidence level) by analyzing CLEO data. The second one is to impose a cut $q^2 \le q^2_{\mathrm{max}}$, thus avoiding the region where the weak annihilation contribution is concentrated. The maximal value of q^2 is $(M_B - M_\pi)^2$, but one must exclude a larger region of phase space, such that the *excluded* contribution to the decay rate at large q^2 (corresponding to a region near the origin in the (P_-, P_+) plane) can be reliably calculated. In our numerical analysis, we will study the effect of a cut $q^2 \le (M_B - M_D)^2$, which satisfies this criterion.

For completeness, we note that even after the weak annihilation contribution near maximum q^2 has been removed, there could in principle exist other, flavor-specific contributions to the semileptonic decay amplitudes that are different for charged and neutral B mesons. The leading

terms of this kind contribute at order $1/m_b$ in the shape-function region and are parameterized by a set of four-quark subleading shape functions [16,31,32]. Model estimates of these contributions show that they are very small for all observables considered for an extraction of $|V_{ub}|$ [32,45]. If only flavor-averaged decay rates are measured, the effects of four-quark subleading shape functions can be absorbed entirely by a redefinition of the functions $\hat{u}(\hat{\omega})$ and $\hat{v}(\hat{\omega})$ [16], without affecting the moment relations in (18).

IV. SHAPE-FUNCTION PARAMETRIZATIONS

Hadronic-physics effects enter the description of inclusive decay rates via nonperturbative shape functions. Perturbation theory cannot tell us much about the local form of these functions, but moments of them are calculable provided that the domain of integration is much larger than $\Lambda_{\rm QCD}$. Since the shape functions contain information about the internal structure of the B meson, knowledge of them relates directly to the determination of the b-quark mass m_b, the kinetic-energy parameter λ_1, and in principle the matrix elements of higher-dimensional operators. Improved measurements of the shape of the $\bar{B} \to X_s\gamma$ photon spectrum will therefore lead directly to a more precise determination of HQET parameters. This argument can be turned around to constrain the leading shape function using knowledge of m_b and λ_1 from other physical processes such as a $b \to c$ moment analysis [46]. We emphasize, however, that there are obviously infinitely many locally different functions that have identical first few moments. In this section we present a few functional forms that can be used to model the shape functions and to fit the current experimental data.

To achieve stringent constraints on the leading shape function a precise definition of the HQET parameters is required. It is a well-known fact that the pole-mass scheme introduces uncontrollable ambiguities. To avoid these uncertainties several short-distance definitions have been proposed, such as the $\overline{\rm MS}$ scheme, the potential-subtraction scheme [47], the $\Upsilon(1S)$ scheme [48], the kinetic scheme [49], or the shape-function scheme [9]. While the decay rates are of course independent of the particular choice, it is advantageous to use a mass scheme that is designed for the physics problem at hand. In the case of inclusive B decays into light particles, this is the shape-function scheme.

A. Models for the leading shape function

Model-independent constraints on the shape function $\hat{S}(\hat{\omega}, \mu_i)$ can be derived by analyzing moments defined with an upper limit of integration $\hat{\omega}_0$, i.e.

$$M_N(\hat{\omega}_0, \mu_i) \equiv \int_0^{\hat{\omega}_0} d\hat{\omega}\, \hat{\omega}^N \hat{S}(\hat{\omega}, \mu_i). \tag{40}$$

For practical applications, $\hat{\omega}_0$ should be taken of order the size of the window where the $\bar{B} \to X_s\gamma$ photon spectrum is experimentally accessible, $\hat{\omega}_0 = M_B - 2E_\gamma^{\rm min}$ with $E_\gamma^{\rm min} \approx 1.8$ GeV. These moments can be expanded in terms of matrix elements of local operators as long as $\hat{\omega}_0$ is large compared to $\Lambda_{\rm QCD}$. In the shape-function scheme, HQET parameters are defined to all orders in perturbation theory through ratios of such moments, e.g. [9]

$$\begin{aligned}
&\frac{M_1(\mu_f + \bar{\Lambda}(\mu_f, \mu_i), \mu_i)}{M_0(\mu_f + \bar{\Lambda}(\mu_f, \mu_i), \mu_i)} = \bar{\Lambda}(\mu_f, \mu_i),\\
&\frac{M_2(\mu_f + \bar{\Lambda}(\mu_f, \mu_i), \mu_i)}{M_0(\mu_f + \bar{\Lambda}(\mu_f, \mu_i), \mu_i)} = \frac{\mu_\pi^2(\mu_f, \mu_i)}{3} + \bar{\Lambda}^2(\mu_f, \mu_i).
\end{aligned} \tag{41}$$

Here, the factorization scale $\mu_f \gg \Lambda_{\rm QCD}$ is related to the size of the integration domain via the implicit equation $\hat{\omega}_0 = \mu_f + \bar{\Lambda}(\mu_f, \mu_i)$. In practice μ_f is close to the intermediate scale μ_i. At tree level, the relations between parameters in the shape-function scheme and the pole scheme are $\bar{\Lambda}(\mu_f, \mu_i) = \bar{\Lambda}^{\rm pole}$ and $\mu_\pi^2(\mu_f, \mu_i) = -\lambda_1$. The corresponding relations at one- and two-loop order have been worked out in [9,50], respectively. These relations allow us to obtain precise determinations of $\bar{\Lambda}(\mu_f, \mu_i)$ and $\mu_\pi^2(\mu_f, \mu_i)$ from other physical processes.

For reference purposes, it is helpful to quote values for $\bar{\Lambda}$ and μ_π^2 using only a single scale μ_* instead of two independent scales μ_f and μ_i. To one-loop order, these parameters can be related to those determined from the moments via [9]

$$\begin{aligned}
\bar{\Lambda}(\mu_*, \mu_*) &= \bar{\Lambda}(\mu_f, \mu_i) + \mu_* \frac{C_F\alpha_s(\mu_*)}{\pi} - \mu_f \frac{C_F\alpha_s(\mu_i)}{\pi}\\
&\quad\times\left[1 - 2\left(1 - \frac{\mu_\pi^2(\mu_f, \mu_i)}{3\mu_f^2}\right)\ln\frac{\mu_f}{\mu_i}\right],\\
\mu_\pi^2(\mu_*, \mu_*) &= \mu_\pi^2(\mu_f, \mu_i)\left[1 + \frac{C_F\alpha_s(\mu_*)}{2\pi} - \frac{C_F\alpha_s(\mu_i)}{\pi}\right.\\
&\quad\left.\times\left(\frac{1}{2} + 3\ln\frac{\mu_f}{\mu_i}\right)\right] + 3\mu_f^2\frac{C_F\alpha_s(\mu_i)}{\pi}\ln\frac{\mu_f}{\mu_i},
\end{aligned} \tag{42}$$

where we have neglected higher-dimensional operator matrix elements that are suppressed by inverse powers of μ_f. A typical choice for the scale μ_* is 1.5 GeV, which we will use as the reference scale throughout this work. It will be convenient to connect the parameter $\bar{\Lambda}$ extracted from the first moment of the shape function with a low-scale subtracted quark-mass definition referred to as the ''shape-function'' mass. Following [9], we define

$$m_b(\mu_f, \mu_i) \equiv M_B - \bar{\Lambda}(\mu_f, \mu_i). \tag{43}$$

The general procedure for modeling the leading shape function $\hat{S}(\hat{\omega}, \mu_i)$ from a given functional form $F(\hat{\omega})$ is as

follows. The shape of $F(\hat{\omega})$ is assumed to be tunable so that it can be used to fit the $\bar{B} \to X_s\gamma$ photon spectrum. Only the norm of the shape function is fixed theoretically. Note that the moment relations (41) are insensitive to the norm, so that formulas for $\bar{\Lambda}$ and μ_π^2 follow directly from the functional form of $F(\hat{\omega})$. Examples of such formulas will be given below. We define moments $M_N^{[F]}(\hat{\omega}_0)$ of F in analogy with (40). The first relation in (41) implies that for a given $\hat{\omega}_0$ the factorization scale is

$$\mu_f = \hat{\omega}_0 - \frac{M_1^{[F]}(\hat{\omega}_0)}{M_0^{[F]}(\hat{\omega}_0)}. \tag{44}$$

Now that μ_f is known, the norm is determined by requiring that the zeroth moment of the shape function is [9]

$$M_0(\hat{\omega}_0, \mu_i) = 1 - \frac{C_F\alpha_s(\mu_i)}{\pi}\left(\ln^2\frac{\mu_f}{\mu_i} + \ln\frac{\mu_f}{\mu_i} + \frac{\pi^2}{24}\right) + \frac{C_F\alpha_s(\mu_i)}{\pi}\left(\ln\frac{\mu_f}{\mu_i} - \frac{1}{2}\right)\frac{\mu_\pi^2(\mu_f, \mu_i)}{3\mu_f^2} + \ldots. \tag{45}$$

It follows that $[M_0(\hat{\omega}_0, \mu_i)/M_0^{[F]}(\hat{\omega}_0)]F(\hat{\omega})$ serves as a model of $\hat{S}(\hat{\omega}, \mu_i)$ or $\hat{S}(\hat{\omega}, \mu_i)$.

We now suggest three two-parameter models for the leading-order shape function based on an exponential-type function $F^{(\mathrm{exp})}$, a Gaussian-type function $F^{(\mathrm{gauss})}$, and hyperbolic-type function $F^{(\mathrm{hyp})}$. We use two parameters that can be tuned to fit the photon spectrum: a dimensionful quantity Λ which coincides with the position of the average $\langle\hat{\omega}\rangle$, and a positive number b which governs the behavior for small $\hat{\omega}$. The functions we propose are

$$F^{(\mathrm{exp})}(\hat{\omega}; \Lambda, b) = \frac{N^{(\mathrm{exp})}}{\Lambda}\left(\frac{\hat{\omega}}{\Lambda}\right)^{b-1}\exp\left(-d_{(\mathrm{exp})}\frac{\hat{\omega}}{\Lambda}\right),$$
$$F^{(\mathrm{gauss})}(\hat{\omega}; \Lambda, b) = \frac{N^{(\mathrm{gauss})}}{\Lambda}\left(\frac{\hat{\omega}}{\Lambda}\right)^{b-1}\exp\left(-d_{(\mathrm{gauss})}\frac{\hat{\omega}^2}{\Lambda^2}\right),$$
$$F^{(\mathrm{hyp})}(\hat{\omega}; \Lambda, b) = \frac{N^{(\mathrm{hyp})}}{\Lambda}\left(\frac{\hat{\omega}}{\Lambda}\right)^{b-1}\cosh^{-1}\left(d_{(\mathrm{hyp})}\frac{\hat{\omega}}{\Lambda}\right). \tag{46}$$

For convenience, we normalize these functions to unity. The parameters $d_{(i)}$ are determined by the choice $\Lambda = \langle\hat{\omega}\rangle$. We find

$$N^{(\mathrm{exp})} = \frac{d_{(\mathrm{exp})}^b}{\Gamma(b)}, \qquad d_{(\mathrm{exp})} = b,$$
$$N^{(\mathrm{gauss})} = \frac{2d_{(\mathrm{gauss})}^{b/2}}{\Gamma(b/2)}, \qquad d_{(\mathrm{gauss})} = \left(\frac{\Gamma(\frac{1+b}{2})}{\Gamma(\frac{b}{2})}\right)^2,$$
$$N^{(\mathrm{hyp})} = \frac{[4d_{(\mathrm{hyp})}]^b}{2\Gamma(b)[\zeta(b, \frac{1}{4}) - \zeta(b, \frac{3}{4})]},$$
$$d_{(\mathrm{hyp})} = \frac{b}{4}\frac{\zeta(1+b, \frac{1}{4}) - \zeta(1+b, \frac{3}{4})}{\zeta(b, \frac{1}{4}) - \zeta(b, \frac{3}{4})}, \tag{47}$$

where $\zeta(b, a) = \sum_{k=0}^{\infty}(k+a)^{-b}$ is the generalized Riemann zeta function. An illustration of the different functional forms is given on the left-hand side in Fig. 2. We show a plot with the choice $b = 2$, corresponding to a linear onset for small $\hat{\omega}$.

For the first two models, analytic expressions for the HQET parameters $\bar{\Lambda}$ and μ_π^2 are available. Following the discussion above, we compute the moments on the interval $[0, \hat{\omega}_0]$ and find for the exponential form $F^{(\mathrm{exp})}(\hat{\omega}; \Lambda, b)$

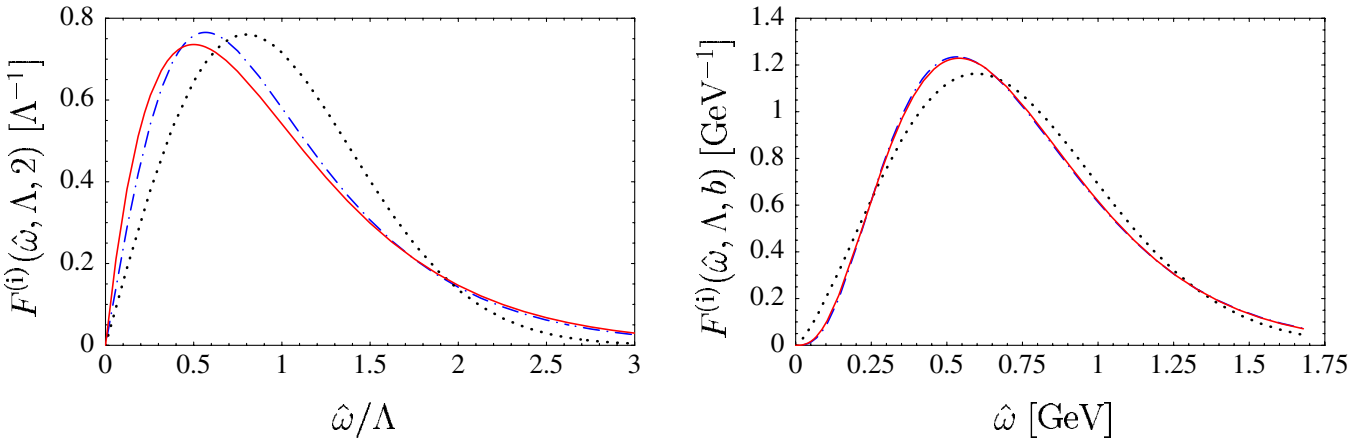

FIG. 2 (color online). LEFT: Different functional forms for the leading shape function. We show $F^{(\mathrm{exp})}(\hat{\omega}, \Lambda, 2)$ (solid), $F^{(\mathrm{gauss})}(\hat{\omega}, \Lambda, 2)$ (dotted), and $F^{(\mathrm{hyp})}(\hat{\omega}, \Lambda, 2)$ (dash-dotted) as functions of the ratio $\hat{\omega}/\Lambda$. RIGHT: The same functions with the parameters Λ and b tuned such that $m_b(\mu_*, \mu_*) = 4.61$ GeV and $\mu_\pi^2(\mu_*, \mu_*) = 0.2$ GeV^2. See text for explanation.

$$\bar{\Lambda}(\mu_f,\mu_i) = \frac{\Lambda}{b}\,\frac{\Gamma(1+b)-\Gamma(1+b,\frac{b\hat{\omega}_0}{\Lambda})}{\Gamma(b)-\Gamma(b,\frac{b\hat{\omega}_0}{\Lambda})},$$
$$\mu_\pi^2(\mu_f,\mu_i) = 3\Bigg[\frac{\Lambda^2}{b^2}\,\frac{\Gamma(2+b)-\Gamma(2+b,\frac{b\hat{\omega}_0}{\Lambda})}{\Gamma(b)-\Gamma(b,\frac{b\hat{\omega}_0}{\Lambda})} - \bar{\Lambda}(\mu_f,\mu_i)^2\Bigg], \tag{48}$$

where $\mu_f = \hat{\omega}_0 - \bar{\Lambda}(\mu_f,\mu_i)$, and $\Gamma(x,y)$ is the incomplete Gamma function. A similar calculation for the Gaussian form $F^{(\mathrm{gauss})}(\hat{\omega};\Lambda,b)$ yields

$$\bar{\Lambda}(\mu_f,\mu_i) = \frac{\Lambda}{\sqrt{d_{(\mathrm{gauss})}}}\,\frac{\Gamma(\frac{1+b}{2})-\Gamma(\frac{1+b}{2},\frac{d_{(\mathrm{gauss})}\hat{\omega}_0^2}{\Lambda^2})}{\Gamma(\frac{b}{2})-\Gamma(\frac{b}{2},\frac{d_{(\mathrm{gauss})}\hat{\omega}_0^2}{\Lambda^2})},$$
$$\mu_\pi^2(\mu_f,\mu_i) = 3\Bigg[\frac{\Lambda^2}{d_{(\mathrm{gauss})}}\,\frac{\Gamma(1+\frac{b}{2})-\Gamma(1+\frac{b}{2},\frac{d_{(\mathrm{gauss})}\hat{\omega}_0^2}{\Lambda^2})}{\Gamma(\frac{b}{2})-\Gamma(\frac{b}{2},\frac{d_{(\mathrm{gauss})}\hat{\omega}_0^2}{\Lambda^2})} - \bar{\Lambda}(\mu_f,\mu_i)^2\Bigg]. \tag{49}$$

The corresponding relations for $F^{(\mathrm{hyp})}(\hat{\omega};\Lambda,b)$ must be obtained numerically.

Ultimately the shape function should be fitted to the $\bar{B}\to X_s\gamma$ photon spectrum, and the above equations then determine $\bar{\Lambda}$ and μ_π^2. On the other hand, these formulas can be inverted to determine Λ and b from the current values of the HQET parameters. For example, if we adopt the values $m_b(\mu_*,\mu_*) = 4.61$ GeV and $\mu_\pi^2(\mu_*,\mu_*) = 0.20\ \mathrm{GeV}^2$ for the parameters in (42) at $\mu_* = 1.5$ GeV, then we find the parameter pair $\Lambda \approx 0.72$ GeV, $b \approx 3.95$ for the exponential model, $\Lambda \approx 0.71$ GeV, $b \approx 2.36$ for the Gaussian model, and $\Lambda \approx 0.73$ GeV, $b \approx 3.81$ for the hyperbolic model. On the right-hand side of Fig. 2 we show these three different functions plotted on the interval $[0,\hat{\omega}_0]$ over which the moment constraints are imposed. While the exponential (solid) and hyperbolic (dash-dotted) curves are barely distinguishable, the Gaussian model has quite different characteristics. It is broader, steeper at the onset, faster to fall off, and the maximum is shifted toward larger $\hat{\omega}$.

An important comment is that, once a two-parameter ansatz is employed, the shape-function parameters (i.e., m_b and μ_π^2) can either be determined from a fit to the entire photon spectrum, or to the first two moments of the spectrum. Both methods are equivalent and should yield consistent results. If they do not, it would be necessary to refine the ansatz for the functional form of the shape function.

In most applications shape functions are needed for arguments $\hat{\omega}$ of order Λ_{QCD}. However, in some cases, like the ideal cut on hadronic invariant mass, $\hat{\omega}$ is required to be as large as M_D, which is much larger than Λ_{QCD}. The large-$\hat{\omega}$ behavior of the shape functions can be computed in a model-independent way using short-distance methods. For the leading shape function, one finds [9]

$$\hat{S}(\hat{\omega}\gg\Lambda_{\mathrm{QCD}},\mu_i) = -\frac{C_F\alpha_s(\mu_i)}{\pi}\,\frac{1}{\hat{\omega}-\bar{\Lambda}}\left(2\ln\frac{\hat{\omega}-\bar{\Lambda}}{\mu_i}+1\right) + \ldots. \tag{50}$$

Note that this radiative tail is negative, implying that the shape function must go through zero somewhere near $\hat{\omega}\sim$ few Λ_{QCD}. For practical purposes, we "glue" the above expression onto models of the nonperturbative shape function starting at $\hat{\omega} = \bar{\Lambda} + \mu_i/\sqrt{e} \approx 1.6$ GeV, where the tail piece vanishes. In this way we obtain a continuous shape-function model with the correct asymptotic behavior. We stress that for applications with a maximal P_+ not larger than about 1.6 GeV the radiative tail of the shape function is never required. This includes all methods for extracting $|V_{ub}|$ discussed later in this work, except for the case of a cut on hadronic invariant mass, $M_X \le M_0$, if M_0 is above 1.6 GeV.

B. Models for subleading shape functions

In the last section we have been guided by the fact that the $\bar{B}\to X_s\gamma$ photon spectrum is at leading power directly determined by the leading shape function. This helped in finding models that have roughly the same shape as the photon spectrum. At the subleading level considered here, however, no such guidance is provided to us. The available information is limited to the tree-level moment relations (18), stating that the norms of the subleading shape functions vanish while their first moments do not. In [16], two classes of models have been proposed, in which the subleading shape functions are "derived" from the leading shape function. A particularly simple choice is

$$\hat{t}(\hat{\omega}) = -\lambda_2\hat{S}'(\hat{\omega}), \qquad \hat{u}(\hat{\omega}) = \frac{2\lambda_1}{3}\hat{S}'(\hat{\omega}), \qquad \hat{v}(\hat{\omega}) = \lambda_2\hat{S}'(\hat{\omega}). \tag{51}$$

Below, we will sometimes refer to this set of functions as the "default choice". We choose the parameter $-\lambda_1$ in the expression for $\hat{u}(\hat{\omega})$ (as well as in the expressions for the second-order hadronic power corrections) to coincide with the quantity $\mu_\pi^2(\mu_f,\mu_i)$ given in (48) and (49). However, for consistency with the tree-level moment relations, we identity the parameter $\bar{\Lambda}$ in (15) and (35) with the quantity $\bar{\Lambda}(\mu_f,\mu_i)$ evaluated in the limit where $\omega_0\to\infty$. This implies $\bar{\Lambda} = \Lambda$ for all three types of functions and ensures that the subleading shape functions have zero norm when integrated over $0 \le \hat{\omega} < \infty$.

There are of course infinitely many possibilities to find models for subleading shape functions that are in accordance with (18). Any function with vanishing norm and first moment can be arbitrarily added to any model for a subleading shape function without violating the moment relations. Several such functions have been proposed in

recent work on subleading shape functions, see e.g. [16,30,32,45]. Specifically, we define the functions

$$h_1(\hat\omega) = \frac{M_2}{N\Omega_0^3}\,\frac{a^{a+1}}{2\Gamma(a)}\,z^{a-1}e^{-az}\Big(\frac{a-1}{z} - a(2-z)\Big),$$
$$h_2(\hat\omega) = \frac{M_2}{N\Omega_0^3}\,\frac{a^3}{2}\,e^{-az}\Big(1 - 2az + \frac{a^2z^2}{2}\Big),$$
$$h_3(\hat\omega) = \frac{M_2}{N\Omega_0^3}\Big\{\Big[\frac{2\sqrt{\pi a}}{\pi-2}e^{-az^2}\Big(1 - 2z\sqrt{\frac{a}{\pi}}\Big)\Big] - 2e^{-z} + 2ze^{-2z}\mathrm{Ei}(z)\Big\},$$
$$h_4(\hat\omega) = \frac{M_2}{N\Omega_0^3}\Big\{\Big[\frac{\pi^2}{4}\,\frac{2\sqrt{\pi a}}{\pi-2}e^{-az^2}\Big(1 - 2z\sqrt{\frac{a}{\pi}}\Big)\Big] + \frac{8}{(1+z^2)^4}\Big[z\ln z + \frac{z}{2}(1+z^2) - \frac{\pi}{4}(1-z^2)\Big]\Big\}, \tag{52}$$

where $z = \hat\omega/\Omega_0$, and the reference quantity $\Omega_0 = O(\Lambda_{\rm QCD})$ depends on the type of function, namely $\Omega_0 = \bar\Lambda$ for h_1 and h_2, $\Omega_0 = \frac{2}{3}\bar\Lambda$ for h_3, and $\Omega_0 = \frac{8}{3\pi}\bar\Lambda$ for h_4. The quantity a is a free parameter. The functions (52) have by construction vanishing norm and first moment. Their second moments are given by the parameter M_2, provided the normalization constants are chosen as $N = 1$ for h_1 and h_2, and

$$N = 1 - \frac{4-\pi}{2(\pi-2)}\,\frac{1}{a}, \qquad N = 1 - \frac{\pi^2(4-\pi)}{8(\pi-2)}\,\frac{1}{a} \tag{53}$$

for h_3 and h_4, respectively. The values for the parameters a and M_2 should be chosen such that the following characteristics of subleading shape functions are respected: First, they are dimensionless functions, so that their values are naturally of $O(1)$ for $\hat\omega \sim \Lambda_{\rm QCD}$. Secondly, when integrated over a sufficiently large domain, their contributions are determined in terms of their first few moments. In particular, this implies that for values of $\hat\omega \gg \Lambda_{\rm QCD}$ the integrals over the subleading shape functions must approach zero. Taking these considerations into account, we use $M_2 = (0.3\text{GeV})^3$ in all cases and choose $a = 3.5$ for h_1, $a = 5$ for h_2, and $a = 10$ for h_3 and h_4.

Given the four functions (52), we can construct several new models for the subleading shape functions $\hat t(\hat\omega)$, $\hat u(\hat\omega)$, and $\hat v(\hat\omega)$. For each function, we construct a set of 9 models by adding or subtracting any of the functions $h_n(\hat\omega)$ to the default choice in (51). Together, this method yields $9^3 = 729$ different sets $\{\hat t_i(\hat\omega), \hat u_j(\hat\omega), \hat v_k(\hat\omega)\}$ with $i, j, k = 1, \ldots, 9$. This large collection of functions will be used to estimate the hadronic uncertainties in our predictions for partial decay rates. Note that for most of these sets we no longer have $\hat t_i(\hat\omega) = -\hat v_k(\hat\omega)$, which was an "accidental" feature of the default model (51). The fact that the two functions have equal (but opposite in sign) first moments does not imply that their higher moments should also be related to each other.

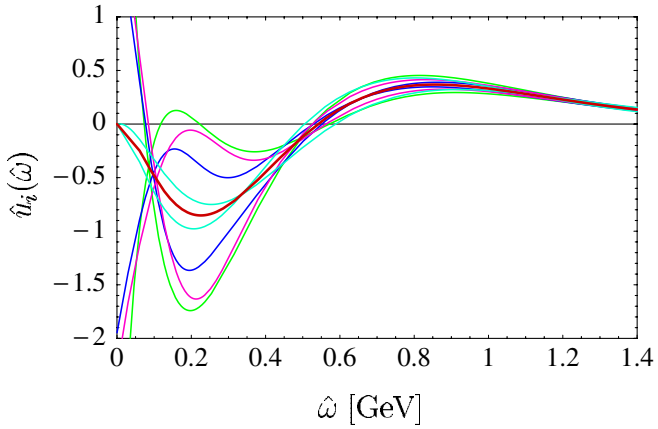

FIG. 3 (color online). Nine models for the subleading shape function $\hat u(\hat\omega)$ obtained by adding or subtracting one of the four functions $h_n(\hat\omega)$ to the default model in (51), shown as the thick central line. See text for explanation.

For the case of $\hat u(\hat\omega)$ the resulting functions are shown in Fig. 3, where we have used the exponential model (46) with parameters $\Lambda = 0.72\,\text{GeV}$ and $b = 3.95$ for the leading shape function. In the region $\hat\omega \sim \Lambda_{\rm QCD}$ they differ dramatically from each other, while the large $\hat\omega$ dependence is dominated by the moment relations (18).

C. Illustrative studies

We stressed several times that the calculation of the hadronic tensor is optimized for the shape-function region of large P_- and small P_+, while it can smoothly be extended over the entire phase space. The notions "large P_-" and "small P_+" are to be understood as the sizes of integration domains for P_- and P_+. Only when the differential distributions are integrated over a sufficiently large region in phase space, global quark-hadron duality ensures that the partonic description used in the present work matches the true, hadronic distributions with good accuracy. A more ambitious goal would be to calculate the differential decay rate point by point in the (P_+, P_-) plane. This can be done invoking local quark-hadron duality, as long as there is a sufficiently large number of hadronic final states contributing to the rate at any given point in phase space.

It is instructive to integrate the triple-differential decay rate (23) over the leptonic variable P_l in the range $P_+ \le P_l \le P_-$, which yields the exact formula

$$\frac{d^2\Gamma_u}{dP_+\,dP_-} = \frac{G_F^2|V_{ub}|^2}{96\pi^3}\,U_y(\mu_h,\mu_i)(M_B - P_+)(P_- - P_+)^2 \times\{(3M_B - 2P_- - P_+)\mathcal{F}_1 + 6(M_B - P_-)\mathcal{F}_2 + (P_- - P_+)\mathcal{F}_3\}. \tag{54}$$

Our theoretical prediction for the double differential decay

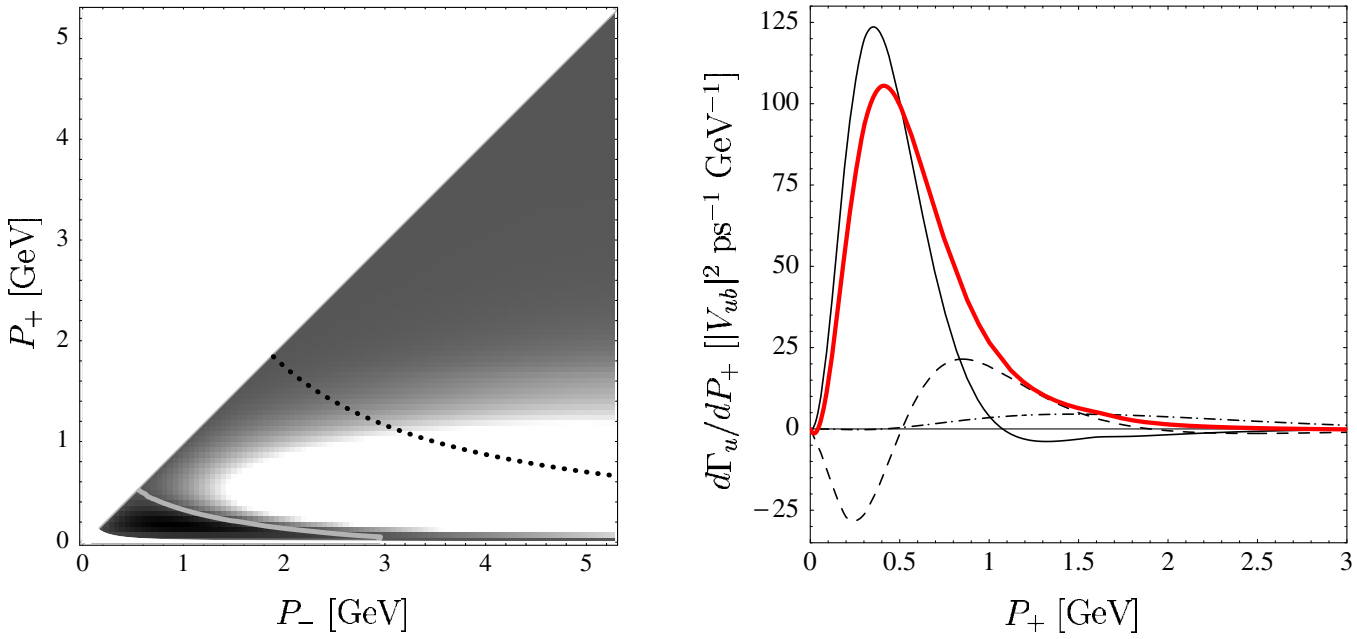

FIG. 4 (color online). LEFT: Theoretical prediction for the double differential decay rate. The light area represents a large decay rate. Black regions denote areas where the decay rate is close to zero. The dotted line is given by $P_+P_- = M_D^2$, which means that charm background is located in the upper wedge. See text for further explanation. RIGHT: The P_+ spectrum extended to large values of P_+. The thin solid line denotes the leading-power prediction, the dashed line depicts first-order power corrections, the dash-dotted line shows second-order power corrections, and the thick solid line is their sum.

rate (54) is shown on the left-hand side of Fig. 4. We use the exponential model for the leading shape function with parameters $m_b(\mu_*, \mu_*) = 4.61$ GeV and $\mu_\pi^2(\mu_*, \mu_*) = 0.2$ GeV^2, as well as the default choice (51) for the subleading shape functions. For very small P_- values the rate turns negative (to the left of the gray line in the figure), signaling a breakdown of quark-hadron duality. It is reassuring that the only region where this happens is the ''resonance region'', where the hadronic invariant mass is of order $\Lambda_{\rm QCD}$, and local duality breaks down.

Another useful quantity to consider is the differential P_+ rate, which is obtained by integrating the double differential rate over P_- in the range $P_+ \le P_- \le M_B$. The resulting P_+ spectrum is shown on the right-hand side of Fig. 4. In the plot we also disentangle the contributions from different orders in power counting.

V. PREDICTIONS AND ERROR ESTIMATES FOR PARTIAL RATES

Before discussing predictions for partial $\bar{B} \to X_u l^- \bar{\nu}$ rates for various kinematical cuts, let us recapitulate the ingredients of the calculation and general procedure. We have presented expressions for the triple-differential decay rate, which can be organized in an expansion in inverse powers of $(M_B - P_+)$. The leading-power contribution is given at next-to-leading order in renormalization-group improved perturbation theory. At first subleading power two contributions arise. The first type involves subleading shape functions and is included at tree evel, while the second type contributes perturbative corrections of order α_s that come with the leading shape function. Further contributions enter at second subleading power and are again of the two types: perturbative corrections of order α_s and nonperturbative structures at tree level. In summary, then, partial rates can be computed term by term in an expansion of the form

$$\Gamma_u = \Gamma_u^{(0)} + (\Gamma_u^{\rm kin(1)} + \Gamma_u^{\rm hadr(1)}) + (\Gamma_u^{\rm kin(2)} + \Gamma_u^{\rm hadr(2)}) + \ldots. \tag{55}$$

The goal of this section is to test the convergence of this series expansion and to perform a thorough analysis of uncertainties. For the kinematical corrections $\Gamma_u^{\rm kin(n)}$ the sum of all terms is known and given by the expressions in (30), while the first two terms in the series correspond to the expanded results in (32) and (33). We will find that in all cases of interest the first two terms give an excellent approximation to the exact result for $\Gamma_u^{\rm kin}$.

For the purpose of illustration, we adopt the exponential model for the shape function and present numerical results for two sets of input parameters, which are biased by the results deduced from fits to $\bar{B} \to X_c l^- \bar{\nu}$ moments [50]. Specifically, we use $m_b(\mu_*, \mu_*) = 4.61$ GeV, $\mu_\pi^2(\mu_*, \mu_*) = 0.2$ GeV^2 (set 1) and $m_b(\mu_*, \mu_*) = 4.55$ GeV, $\mu_\pi^2(\mu_*, \mu_*) = 0.3$ GeV^2 (set 2). The values of the b-quark mass coincide with those obtained at two-loop and one-loop order in [50] (see also the discussion below),

while the values of μ_π^2 are close to the corresponding values in that reference. As was mentioned before, in the future the leading shape function $\hat{S}(\hat{\omega}, \mu_i)$ should be extracted from a fit to the $\bar{B} \to X_s\gamma$ photon spectrum, in which case the uncertainty in its shape becomes an experimental error, which can be systematically reduced with improved data. In the process, the "theoretically preferred" parameter values used in the present work will be replaced with the "true" values extracted directly from data. While this will change the central values for the partial rates, our estimates of the theoretical errors will only be affected marginally.

The different sources of theoretical uncertainties are as follows: First, there are uncertainties associated with the functional forms of the subleading shape functions. To estimate them, we take the spread of results obtained when using the large set of different models described in Sec. IV B, while the central value for a partial decay rate corresponds to the default model (51). Secondly, there are perturbative uncertainties associated with the choice of the matching scales μ_h, μ_i, and $\bar{\mu}$. Decay rates are formally independent of these scales, but a residual dependence remains because of the truncation of the perturbative series. Our error analysis is as follows:

(i) The hard scale μ_h is of order m_b. In perturbative logarithms the scale appears in the combination (ym_b/μ_h), see e.g. (29). To set a central value for μ_h we are guided by the average $\langle y\rangle m_b$. The leading term for the double differential decay rate $d^2\Gamma_u/dP_+dy$ is proportional to $2y^2(3-2y)$. It follows that the average y on the interval $[0, 1]$ is 0.7. However, in some applications y is not integrated over the full domain. Also, there are large negative constants in the matching correction H_{u1} in (29), whose effect can be ameliorated by lowering the scale further. In the error analysis we use the central value of $\mu_h = m_b/2 \approx 2.3$ GeV and vary the scale by a factor between $1/\sqrt{2}$ and $\sqrt{2}$. For the central value $\alpha_s(\mu_h) \approx 0.286$.

(ii) The intermediate scale $\mu_i \sim \sqrt{m_b\Lambda_{\rm QCD}}$ serves as the renormalization point for the jet and shape functions. We fix this scale to $\mu_i = 1.5$ GeV. Variations of μ_i would affect both the normalization and the functional form of the shape function, as determined by the solution to the renormalization-group equation for the shape function discussed in [9,11]. In practice, effects on the shape are irrelevant because the shape function is fitted to data. The only place where the intermediate scale has a direct impact on the extraction of $|V_{ub}|$ is through the normalization of the shape function (45). In the analysis we therefore estimate the uncertainty by assigning the value $\pm(\alpha_s(\mu_i)/\pi)^2$ as a relative error, where $\alpha_s(\mu_i) \approx 0.354$.

(iii) The scale $\bar{\mu}$ appears as the argument of α_s in the perturbative contributions $\Gamma_u^{\rm kin}$. We vary $\bar{\mu}$ from $\mu_i/\sqrt{2}$ to $\sqrt{2}\mu_i$ with the central value $\bar{\mu} = \mu_i = 1.5$ GeV.

These three errors are added in quadrature and assigned as the total perturbative uncertainty. Finally, we need to estimate the effects from higher-dimensional operators at third and higher-order in power counting. If the considered cut includes the region of phase space near the origin ($P_+ \sim P_- \sim \Lambda_{\rm QCD}$), then the dominant such contributions are weak annihilation effects, which we have discussed in Sec. III E. From the analysis in [44] one can derive a bound on the weak annihilation contribution that is $\pm 1.8\%$ of the total decay rate, for which we take $\Gamma_u \approx 70|V_{ub}|^2{\rm ps}^{-1}$ (see below). The resulting uncertainty $\delta\Gamma_u^{\rm WA} = \pm 1.3|V_{ub}|^2{\rm ps}^{-1}$ affects all partial rates which include the region near the origin in the (P_+, P_-) plane. The uncertainty from weak annihilation can be avoided by imposing a cut $q^2 \le q^2_{\rm max}$ (see Sec. V F). For all observables considered in the present work, other power corrections of order $1/m_b^3$ can be safely neglected. This can be seen by multiplying the contributions from second-order hadronic power corrections to the various decay rates (called $\Gamma_u^{\rm hadr(2)}$) by an additional suppression factor $\Lambda_{\rm QCD}/m_b \sim 0.1$.

The following subsection contains a discussion of the total decay rate. In the remainder of this section we then present predictions for a variety of kinematical cuts designed to eliminate (or reduce) the charm background. These partial rates can be computed either numerically or, in many cases, semianalytically. In Appendix B we discuss how to perform the integrations over the kinematical variables P_l and P_- analytically.

A. Total decay rate

Before presenting our predictions for the various partial decay rates, it is useful to have an expression for the total $\bar{B} \to X_u l^- \bar{\nu}$ decay rate expressed in terms of the heavy-quark parameters defined in the shape-function scheme. We start from the exact two-loop expression for the total rate derived in [51], add the second-order hadronic power corrections, which are known at tree level [12,13], and finally convert the parameters m_b and λ_1 from the pole scheme to the shape-function scheme. The relevant replacements at two-loop order can be taken from [50] and read

$$\begin{aligned} m_b^{\rm pole} &= m_b + 0.424\mu_*\alpha_s(\mu)\Big[1 + \Big(1.357 + 1.326\ln\frac{\mu}{\mu_*} \\ &\quad + 0.182\,\frac{\mu_\pi^2}{\mu_*^2}\Big)\alpha_s(\mu)\Big] \\ &\quad + \frac{3\lambda_2 - \mu_\pi^2 - 0.330\mu_*^2\alpha_s^2(\mu)}{2m_b} + \ldots, \\ -\lambda_1 &= \mu_\pi^2 + 0.330\mu_*^2\alpha_s^2(\mu) + \ldots, \end{aligned} \tag{56}$$

where here and from now on $m_b \equiv m_b(\mu_*, \mu_*)$ and $\mu_\pi^2 \equiv \mu_\pi^2(\mu_*, \mu_*)$ are defined in the shape-function scheme. At a reference scale $\mu_* = 1.5$ GeV the values of these parameters have been determined to be $m_b = (4.61 \pm 0.08)$ GeV and $\mu_\pi^2 = (0.15 \pm 0.07)$ GeV^2 [50],[3] where we account for the small $1/m_b$ correction to the relation for the pole mass in the above formula (corresponding to a shift of about -0.02 GeV in m_b), which was not included in that paper.

The resulting expression for the total decay rate is

$$\Gamma_u = \frac{G_F^2 |V_{ub}|^2 m_b^5}{192\pi^3}\Bigg\{1 + \alpha_s(\mu)\Big(-0.768 + 2.122\frac{\mu_*}{m_b}\Big) + \alpha_s^2(\mu)\Bigg[-2.158 + 1.019\ln\frac{m_b}{\mu} + \Big(1.249 + 2.814\ln\frac{\mu}{\mu_*} + 0.386\frac{\mu_\pi^2}{\mu_*^2}\Big)\frac{\mu_*}{m_b} + 0.811\frac{\mu_*^2}{m_b^2}\Bigg] - \frac{3(\mu_\pi^2 - \lambda_2)}{m_b^2} + \ldots\Bigg\}. \tag{57}$$

We observe that for $\mu_* \approx 1.5$ GeV and $\mu = O(m_b)$, the perturbative expansion coefficients are strongly reduced compared to their values in the pole scheme (-0.768 and -2.158, respectively), indicating a vastly improved convergence of the perturbative expansion. For $m_b = \mu = 4.61$ GeV, and $\mu_\pi^2 = 0.15$ GeV^2 we obtain for the one-loop, two-loop, and power corrections inside the brackets in (57): $\{1 - 0.017 - 0.030 - 0.004\}$. All of these are very small corrections to the leading term.

Including the uncertainties in the values of m_b and μ_π^2 quoted above, and varying the renormalization scale μ between m_b and $m_b/2$ (with a central value of $m_b/\sqrt{2}$), we get

$$\frac{\Gamma_u}{|V_{ub}|^2\ \text{ps}^{-1}} = 68.0^{+5.9}_{-5.5}[m_b] \mp 0.7[\mu_\pi^2]^{+0.6}_{-0.9}[\mu] = (68.0 \mp 0.7[\mu_\pi^2]^{+0.6}_{-0.9}[\mu])\Big(\frac{m_b}{4.61\ \text{GeV}}\Big)^{4.81}. \tag{58}$$

Here and below, we quote values for decay rates in units of $|V_{ub}|^2\text{ps}^{-1}$. To convert these results to partial branching fractions the numbers need to be multiplied by the average B-meson lifetime. Without including the two-loop corrections, the central value in the above estimate increases to 70.6. For comparison, with the same set of input parameters our new approach based on (23) predicts a total decay rate of $\Gamma_u = (71.4^{+6.2}_{-5.0} \pm 0.5)|V_{ub}|^2\text{ps}^{-1}$, where the first error accounts for perturbative uncertainties while the second one refers to the modeling of subleading shape functions (to which there is essentially no sensitivity at all in the total rate). The fact that this is in excellent agreement with the direct calculation using (57) supports the notion that the formalism developed in this work can be used to describe arbitrary $\bar{B} \to X_u l^- \bar{\nu}$ decay distributions, both in the shape-function region and in the OPE region of phase space.

[3]The values obtained from a one-loop analysis are $m_b = (4.55 \pm 0.08)$ GeV and $\mu_\pi^2 = (0.34 \pm 0.07)$ GeV^2.

B. Cut on charged-lepton energy

Traditionally, the most common variable to discriminate against the charm background is the charged-lepton energy E_l. As long as one requires that E_l is bigger than $(M_B^2 - M_D^2)/2M_B \approx 2.31$ GeV, the final hadronic state cannot have an invariant mass larger than M_D. For this ideal cut, and using the default set of subleading shape functions, we find

$$\Gamma_u^{(0)} + (\Gamma_u^{\text{kin}(1)} + \Gamma_u^{\text{hadr}(1)}) + (\Gamma_u^{\text{kin}(2)} + \Gamma_u^{\text{hadr}(2)}) = [6.810 + (0.444 - 3.967) + (0.042 - 0.555)]|V_{ub}|^2\text{ps}^{-1}. \tag{59}$$

The corrections from subleading shape functions are quite sizable, in accordance with the findings in [28–30]. Note that the sum $\Gamma_u^{\text{kin}(1)} + \Gamma_u^{\text{kin}(2)} = 0.486$ is an excellent approximation to the exact result $\Gamma_u^{\text{kin}} = 0.482$ (all in units of $|V_{ub}|^2\text{ps}^{-1}$) obtained using (30), indicating that the expansion of the kinematical power corrections is converging rapidly. The same will be true for all other observables considered below.

In practice, the cut on E_l can be relaxed to some extent because the background is well understood, thereby increasing the efficiency and reducing the impact of theoretical uncertainties. Our findings for different values of the cut E_0 are summarized in Table I. Here and below, the

TABLE I. Partial decay rate $\Gamma_u(E_0)$ for a cut on charged-lepton energy $E_l > E_0$ in the B-meson rest frame, given in units of $|V_{ub}|^2\text{ps}^{-1}$. Predictions are based on the shape-function parameter values $m_b = 4.61$ GeV, $\mu_\pi^2 = 0.2$ GeV^2 (top) and $m_b = 4.55$ GeV, $\mu_\pi^2 = 0.3$ GeV^2 (bottom).

E_0 [GeV]	Mean	Subleading SF	Perturbative	Total
1.9	24.79	± 0.53	$^{+1.90}_{-1.66}$	$^{+2.34}_{-2.15}$
2.0	18.92	± 0.60	$^{+1.35}_{-1.20}$	$^{+1.95}_{-1.84}$
2.1	13.07	± 0.71	$^{+0.82}_{-0.75}$	$^{+1.66}_{-1.63}$
2.2	7.59	± 0.81	$^{+0.38}_{-0.34}$	$^{+1.55}_{-1.54}$
2.3	3.12	± 0.89	$^{+0.15}_{-0.16}$	$^{+1.55}_{-1.55}$
2.4	0.42	± 1.05	$^{+0.16}_{-0.22}$	$^{+1.65}_{-1.65}$
1.9	21.10	± 0.53	$^{+1.57}_{-1.35}$	$^{+2.08}_{-1.92}$
2.0	15.83	± 0.60	$^{+1.08}_{-0.94}$	$^{+1.77}_{-1.68}$
2.1	10.73	± 0.68	$^{+0.64}_{-0.55}$	$^{+1.57}_{-1.54}$
2.2	6.12	± 0.74	$^{+0.31}_{-0.23}$	$^{+1.50}_{-1.48}$
2.3	2.47	± 0.84	$^{+0.17}_{-0.22}$	$^{+1.53}_{-1.53}$
2.4	0.29	± 0.99	$^{+0.18}_{-0.24}$	$^{+1.61}_{-1.62}$

columns have the following meaning: "Mean" denotes the prediction for the partial decay rate, "Subleading SF" the uncertainty from subleading shape functions, and "Perturbative" the total perturbative uncertainty. In the column "Total" we add the stated errors plus the uncertainty from weak annihilation in quadrature.

Experiments often do not measure the partial rates in the B-meson rest frame, but in the rest frame of the $\Upsilon(4S)$ resonance produced in e^+e^- collisions. Boosting to the $\Upsilon(4S)$ frame with $\beta = v/c \approx 0.064$ has a small effect on the spectrum and rates. The exact formula for this boost is [20]

$$\gamma\Gamma_u^{(\Upsilon)}(E_0) = \frac{1}{\beta_+ - \beta_-}\int_{\beta_- E_0}^{M_B/2} dE \frac{d\Gamma_u^{(B)}}{dE} \times \left[\beta_+ - \max\left(\beta_-, \frac{E_0}{E}\right)\right], \tag{60}$$

where $\beta_\pm = \sqrt{1 \pm \beta}/\sqrt{1 \mp \beta}$, and the factor $\gamma = 1/\sqrt{1-\beta^2} \approx 1.002$ on the left-hand side takes the time dilation of the B-meson lifetime $\tau_B' = \gamma\tau_B$ into account. (In other words, branching fractions are Lorentz invariant.) The above formula can be accurately approximated by the first term in an expansion in β^2, which yields [20]

$$\gamma\Gamma_u^{(\Upsilon)}(E_0) = \Gamma_u^{(B)}(E_0) - \frac{\beta^2}{6}E_0^3\left[\frac{d}{dE}\frac{1}{E}\frac{d\Gamma_u^{(B)}}{dE}\right]_{E=E_0} + O(\beta^4), \tag{61}$$

as long as E_0 is not too close to the kinematical endpoint (i.e., $E_0 \le \beta_- M_B/2 \approx 2.47$ GeV). The numerical results for the partial decay rate $\gamma\Gamma_u^{(\Upsilon)}(E_0)$ in the rest frame of the $\Upsilon(4S)$ resonance are given in Table II.

TABLE II. Same as Table I, but for the partial decay rate $\gamma\Gamma_u^{(\Upsilon)}(E_0)$ for a cut on lepton energy $E_l > E_0$ in the $\Upsilon(4S)$ rest frame.

E_0 [GeV]	Mean	Subleading SF	Perturbative	Total
1.9	24.82	± 0.54	$^{+1.91}_{-1.66}$	$^{+2.35}_{-2.15}$
2.0	19.00	± 0.61	$^{+1.37}_{-1.21}$	$^{+1.96}_{-1.85}$
2.1	13.25	± 0.71	$^{+0.85}_{-0.76}$	$^{+1.68}_{-1.63}$
2.2	7.99	± 0.78	$^{+0.42}_{-0.37}$	$^{+1.54}_{-1.53}$
2.3	3.83	± 0.86	$^{+0.18}_{-0.13}$	$^{+1.54}_{-1.53}$
2.4	1.31	± 0.99	$^{+0.10}_{-0.14}$	$^{+1.61}_{-1.61}$
1.9	21.16	± 0.54	$^{+1.58}_{-1.35}$	$^{+2.09}_{-1.93}$
2.0	15.94	± 0.60	$^{+1.10}_{-0.95}$	$^{+1.78}_{-1.69}$
2.1	10.94	± 0.68	$^{+0.66}_{-0.57}$	$^{+1.58}_{-1.54}$
2.2	6.49	± 0.74	$^{+0.34}_{-0.26}$	$^{+1.50}_{-1.48}$
2.3	3.05	± 0.84	$^{+0.17}_{-0.18}$	$^{+1.53}_{-1.53}$
2.4	0.98	± 0.92	$^{+0.13}_{-0.18}$	$^{+1.56}_{-1.57}$

Cut on hadronic P_+

Cutting on P_+ samples the same hadronic phase space as a cut on the charged-lepton energy, but with much better efficiency [9,14]. The phase space $P_+ \le \Delta_P$ with the ideal separator $\Delta_P = M_D^2/M_B \approx 0.66$ GeV contains well over half of all $\bar{B} \to X_u l^- \bar{\nu}$ events. Here we find with the default settings

$$\begin{aligned}\Gamma_u^{(0)} + (\Gamma_u^{\mathrm{kin}(1)} + \Gamma_u^{\mathrm{hadr}(1)}) + (\Gamma_u^{\mathrm{kin}(2)} + \Gamma_u^{\mathrm{hadr}(2)}) \\ = [53.225 + (4.646 - 11.862) + (0.328 \\ - 0.227)]|V_{ub}|^2\mathrm{ps}^{-1}.\end{aligned} \tag{62}$$

We see a much better convergence of the power series than in the case of a cut on the charged-lepton energy, namely $53.225 - 7.216 - 0.100$ when grouping the above numbers according to their power counting. Once again, the sum $\Gamma_u^{\mathrm{kin}(1)} + \Gamma_u^{\mathrm{kin}(2)} = 4.973$ is very close to the full kinematical correction $\Gamma_u^{\mathrm{kin}} = 4.959$ (in units of $|V_{ub}|^2\mathrm{ps}^{-1}$).

Often times it is required to impose an additional cut on the charged-lepton energy, as leptons that are too soft are difficult to detect. In Table III we list results for both $E_l \ge 0$ and $E_l \ge 1.0$ GeV. For the ideal cut we find that the

TABLE III. Partial decay rate $\Gamma_u(\Delta_P, E_0)$ for a cut on the hadronic variable $P_+ \le \Delta_P$ and lepton energy $E_l \ge E_0$, given in units of $|V_{ub}|^2\mathrm{ps}^{-1}$. Predictions are based on the shape-function parameter values $m_b = 4.61$ GeV, $\mu_\pi^2 = 0.2$ GeV^2 (top) and $m_b = 4.55$ GeV, $\mu_\pi^2 = 0.3$ GeV^2 (bottom).

Δ_P [GeV]	E_0 [GeV]	Mean	Subl. SF	Pert.	Total
0.70	0.0	48.90	± 1.15	$^{+2.83}_{-2.65}$	$^{+3.30}_{-3.15}$
0.65	0.0	45.34	± 1.46	$^{+2.55}_{-2.41}$	$^{+3.20}_{-3.09}$
0.60	0.0	41.34	± 1.76	$^{+2.26}_{-2.15}$	$^{+3.13}_{-3.05}$
0.55	0.0	36.91	± 2.01	$^{+1.95}_{-1.87}$	$^{+3.08}_{-3.02}$
0.50	0.0	32.09	± 2.34	$^{+1.64}_{-1.58}$	$^{+3.12}_{-3.09}$
0.70	1.0	43.36	± 1.02	$^{+2.54}_{-2.39}$	$^{+3.01}_{-2.88}$
0.65	1.0	40.18	± 1.30	$^{+2.28}_{-2.16}$	$^{+2.92}_{-2.82}$
0.60	1.0	36.59	± 1.59	$^{+2.01}_{-1.92}$	$^{+2.86}_{-2.80}$
0.55	1.0	32.61	± 1.86	$^{+1.73}_{-1.67}$	$^{+2.84}_{-2.80}$
0.50	1.0	28.29	± 2.19	$^{+1.44}_{-1.40}$	$^{+2.91}_{-2.89}$
0.70	0.0	39.95	± 1.19	$^{+2.18}_{-2.06}$	$^{+2.79}_{-2.70}$
0.65	0.0	36.94	± 1.42	$^{+1.95}_{-1.86}$	$^{+2.72}_{-2.66}$
0.60	0.0	33.67	± 1.65	$^{+1.71}_{-1.65}$	$^{+2.69}_{-2.65}$
0.55	0.0	30.15	± 1.88	$^{+1.47}_{-1.43}$	$^{+2.70}_{-2.68}$
0.50	0.0	26.40	± 2.09	$^{+1.22}_{-1.21}$	$^{+2.73}_{-2.72}$
0.70	1.0	35.42	± 1.13	$^{+1.95}_{-1.85}$	$^{+2.59}_{-2.51}$
0.65	1.0	32.73	± 1.34	$^{+1.74}_{-1.66}$	$^{+2.53}_{-2.48}$
0.60	1.0	29.81	± 1.55	$^{+1.52}_{-1.47}$	$^{+2.51}_{-2.48}$
0.55	1.0	26.65	± 1.76	$^{+1.29}_{-1.27}$	$^{+2.52}_{-2.51}$
0.50	1.0	23.29	± 1.95	$^{+1.07}_{-1.06}$	$^{+2.56}_{-2.55}$

prediction is quite precise, as the total theoretical uncertainty is only about 6.8%. For comparison, the ideal cut for the lepton energy is uncertain by about 50%, but rapidly improving as the energy cut is relaxed.

D. Cut on hadronic invariant mass and q^2

The most efficient separator for the discrimination of $\bar{B} \to X_c l^- \bar{\nu}$ events is a cut on the invariant mass M_X of the hadronic final state, $M_X \le M_D$ [52,53]. It has also been argued [54] that a cut on q^2 can reduce the shape-function sensitivity, since it avoids the collinear region in phase space where $P_- \gg P_+$. In order to optimize signal efficiency and theoretical uncertainties, it was suggested in [55] to combine a q^2 cut with a cut on hadronic invariant mass.

The theoretical predictions obtained in [54,55] were based on a conventional OPE calculation, which was assumed to be valid for these cuts. The assessment of the shape-function sensitivity was based on convolving the tree-level decay rate with a "tree-level shape function", for which two models (a realistic model similar to the ones considered here, and an unrealistic δ-function model) were employed. The shape-function sensitivity was then inferred from the comparison of the results obtained with the two models. The sensitivity to subleading shape functions was not considered, since it was assumed to be very small. Since our formalism smoothly interpolates between the "shape-function" and "OPE" regions, and since we include radiative corrections as well as power corrections as far as they are known, we can estimate the sensitivity of a combined M_X–q^2 cut to the leading and subleading shape functions much more accurately. Contrary to [55], we do not find a significant reduction of the shape-function sensitivity when adding the q^2 cut to a cut on hadronic invariant mass.

In Table IV we give results for typical cuts on M_X and q^2, with and without including an additional cut on charged-lepton energy. Let us study the contributions for the optimal cut $M_X \le M_D$ in detail. We find with the default settings

$$\begin{aligned}\Gamma_u^{(0)} + (\Gamma_u^{\mathrm{kin}(1)} + \Gamma_u^{\mathrm{hadr}(1)}) + (\Gamma_u^{\mathrm{kin}(2)} + \Gamma_u^{\mathrm{hadr}(2)}) \\ = [58.541 + (8.027 - 9.048) + (2.100 \\ - 0.318)]|V_{ub}|^2\mathrm{ps}^{-1}. \end{aligned} \quad (63)$$

Note the almost perfect (accidental) cancellation of the two terms at order $1/m_b$. The resulting power series, $58.541 - 1.022 + 1.782$, again exhibits good convergence. As previously, the sum $\Gamma_u^{\mathrm{kin}(1)} + \Gamma_u^{\mathrm{kin}(2)} = 10.127$ is a good approximation to the exact value $\Gamma_u^{\mathrm{kin}} = 9.753$ (in units of $|V_{ub}|^2\mathrm{ps}^{-1}$). The analogous analysis for a combined cut $M_X \le 1.7$ GeV and $q^2 \ge 8.0$ GeV^2 reads

TABLE IV. Partial decay rate $\Gamma_u(M_0, q_0^2, E_0)$ for combined cuts $M_X \le M_0$ on hadronic invariant mass, $q^2 > q_0^2$ on leptonic invariant mass, and $E_l \ge E_0$ on charged-lepton energy, given in units of $|V_{ub}|^2\mathrm{ps}^{-1}$. Predictions are based on the shape-function parameter values $m_b = 4.61$ GeV, $\mu_\pi^2 = 0.2$ GeV^2 (top) and $m_b = 4.55$ GeV, $\mu_\pi^2 = 0.3$ GeV^2 (bottom).

M_0 [GeV]	q_0^2[GeV^2]	E_0 [GeV]	Mean	Subl. SF	Pert.	Total
M_D	0.0	0.0	59.30	± 0.36	$^{+4.22}_{-3.73}$	$^{+4.42}_{-3.96}$
1.70	0.0	0.0	53.13	± 0.73	$^{+3.67}_{-3.31}$	$^{+3.95}_{-3.61}$
1.55	0.0	0.0	45.72	± 1.16	$^{+3.11}_{-2.84}$	$^{+3.55}_{-3.32}$
M_D	6.0	0.0	34.37	± 0.37	$^{+2.97}_{-2.58}$	$^{+3.25}_{-2.89}$
1.70	8.0	0.0	24.80	± 0.36	$^{+2.24}_{-1.98}$	$^{+2.59}_{-2.37}$
M_D	$(M_B - M_D)^2$	0.0	12.55	± 0.49	$^{+1.41}_{-1.24}$	$^{+1.95}_{-1.83}$
M_D	0.0	1.0	53.49	± 0.36	$^{+3.91}_{-3.45}$	$^{+4.13}_{-3.69}$
1.70	0.0	1.0	48.25	± 0.63	$^{+3.42}_{-3.08}$	$^{+3.70}_{-3.38}$
1.55	0.0	1.0	41.81	± 1.03	$^{+2.91}_{-2.66}$	$^{+3.34}_{-3.12}$
M_D	6.0	1.0	33.88	± 0.37	$^{+2.94}_{-2.55}$	$^{+3.22}_{-2.87}$
1.70	8.0	1.0	24.74	± 0.36	$^{+2.23}_{-1.97}$	$^{+2.59}_{-2.37}$
M_D	$(M_B - M_D)^2$	1.0	12.55	± 0.49	$^{+1.41}_{-1.24}$	$^{+1.95}_{-1.83}$
M_D	0.0	0.0	50.08	± 0.54	$^{+3.52}_{-3.11}$	$^{+3.78}_{-3.40}$
1.70	0.0	0.0	44.20	± 0.86	$^{+2.98}_{-2.69}$	$^{+3.35}_{-3.09}$
1.55	0.0	0.0	37.76	± 1.22	$^{+2.46}_{-2.26}$	$^{+3.03}_{-2.86}$
M_D	6.0	0.0	29.42	± 0.35	$^{+2.50}_{-2.16}$	$^{+2.82}_{-2.52}$
1.70	8.0	0.0	20.87	± 0.39	$^{+1.84}_{-1.61}$	$^{+2.26}_{-2.08}$
M_D	$(M_B - M_D)^2$	0.0	10.49	± 0.48	$^{+1.16}_{-1.00}$	$^{+1.76}_{-1.68}$
M_D	0.0	1.0	45.29	± 0.50	$^{+3.27}_{-2.88}$	$^{+3.54}_{-3.18}$
1.70	0.0	1.0	40.22	± 0.77	$^{+2.78}_{-2.50}$	$^{+3.15}_{-2.90}$
1.55	0.0	1.0	34.55	± 1.09	$^{+2.31}_{-2.11}$	$^{+2.85}_{-2.69}$
M_D	6.0	1.0	28.99	± 0.34	$^{+2.48}_{-2.13}$	$^{+2.80}_{-2.50}$
1.70	8.0	1.0	20.82	± 0.39	$^{+1.83}_{-1.60}$	$^{+2.26}_{-2.08}$
M_D	$(M_B - M_D)^2$	1.0	10.49	± 0.48	$^{+1.16}_{-1.00}$	$^{+1.78}_{-1.68}$

$$\begin{aligned}\Gamma_u^{(0)} + (\Gamma_u^{\mathrm{kin}(1)} + \Gamma_u^{\mathrm{hadr}(1)}) + (\Gamma_u^{\mathrm{kin}(2)} + \Gamma_u^{\mathrm{hadr}(2)}) \\ = [25.880 + (4.049 - 6.358) + (1.399 \\ - 0.171)]|V_{ub}|^2\mathrm{ps}^{-1}, \end{aligned} \quad (64)$$

which means that the power series is $25.880 - 2.309 + 1.228$. Here we have $\Gamma_u^{\mathrm{kin}(1)} + \Gamma_u^{\mathrm{kin}(2)} = 5.449$, which is close to $\Gamma_u^{\mathrm{kin}} = 5.160$ (in units of $|V_{ub}|^2\mathrm{ps}^{-1}$).

E. Cut on $s_H^{\max}$ and E_l

In [56], the *BABAR* collaboration employed a cut on both $E_l \ge E_0$ and a new kinematical variable $s_H^{\max} \le s_0$, where the definition for $s_H^{\max}$ involves both hadronic and leptonic variables. In the B-meson rest frame, it is

$$s_H^{\max} = M_B^2 + q^2 - 2M_B\left(E_l + \frac{q^2}{4E_l}\right). \quad (65)$$

TABLE V. Partial decay rate $\Gamma_u(s_0, E_0)$ for combined cuts $s_H^{\max} \le s_0$ and $E_l \ge E_0$, given in units of $|V_{ub}|^2 \mathrm{ps}^{-1}$. Predictions are based on the shape-function parameter values $m_b = 4.61$ GeV, $\mu_\pi^2 = 0.2$ GeV^2 (top) and $m_b = 4.55$ GeV, $\mu_\pi^2 = 0.3$ GeV^2 (bottom).

s_0[GeV^2]	E_0 [GeV]	Mean	Subl. SF	Pert.	Total
3.5	1.8	17.39	± 0.62	$^{+1.54}_{-1.36}$	$^{+2.08}_{-1.96}$
3.5	1.9	15.86	± 0.63	$^{+1.33}_{-1.18}$	$^{+1.94}_{-1.84}$
3.5	2.0	13.70	± 0.66	$^{+1.05}_{-0.94}$	$^{+1.77}_{-1.71}$
3.5	2.1	10.78	± 0.73	$^{+0.71}_{-0.64}$	$^{+1.62}_{-1.59}$
3.5	1.8	14.57	± 0.60	$^{+1.25}_{-1.09}$	$^{+1.87}_{-1.77}$
3.5	1.9	13.18	± 0.61	$^{+1.06}_{-0.92}$	$^{+1.76}_{-1.68}$
3.5	2.0	11.28	± 0.64	$^{+0.82}_{-0.71}$	$^{+1.63}_{-1.58}$
3.5	2.1	8.77	± 0.69	$^{+0.54}_{-0.46}$	$^{+1.54}_{-1.51}$

Rewriting the phase space of this cut in the variables P_+, P_-, P_l, we find

$$\begin{aligned} &0 \le P_+ \le \min(M_B - 2E_0, \sqrt{s_0}), \\ &P_+ \le P_- \le \min\left(\frac{s_0}{P_+}, M_B\right), \\ &P_+ \le P_l \le \min(M_B - 2E_0, P_-), \end{aligned} \tag{66}$$

where it is understood that if $q^2 = (M_B - P_+) \times (M_B - P_-) \le (M_B - \sqrt{s_0})^2$, then the interval $P_l^{\min} < P_l < P_l^{\max}$ must be *excluded* from the P_l integration. Here

$$P_l^{\max/\min}(P_+, P_-) = \left(\frac{P_+ + P_-}{2} + \frac{s_0 - P_+P_-}{2M_B}\right) \pm \sqrt{\left(\frac{P_+ + P_-}{2} + \frac{s_0 - P_+P_-}{2M_B}\right)^2 - s_0}. \tag{67}$$

A summary of our findings is given in Table V. When compared to the pure charged-lepton energy cut in Table I, the additional cut on $s_H^{\max}$ eliminates roughly another 20%–30% of events. However, the hope is that this cut also reduces the sensitivity to the leading shape function, which we expect to be sizable for the pure E_l cut. The uncertainty from subleading shape functions, however, is almost unaffected by the $s_H^{\max}$ cut.

F. Eliminating weak annihilation contributions

In Sec. III E we have argued that a cut on *high* q^2, i.e., $q^2 < q_0^2$, will eliminate the effect of weak annihilation and remove the uncertainty associated with this contribution. The cutoff q_0^2 should be small enough to exclude the region around $q^2 = m_b^2$, where this contribution is concentrated. It is instructive to assess the "cost" of such an additional cut in terms of the loss of efficiency and, more importantly, the behavior of the remaining uncertainties. In order to do this, we combine the cut $q^2 \le (M_B - M_D)^2$ with either a cut on P_+ or on M_X. While this particular choice for q_0^2 still leaves some room to improve the efficiency by increasing q_0^2, it is not desirable to raise the cut much further, since this would threaten the validity of quark-hadron duality.

TABLE VI. Examples of partial decay rates with a cut on $q^2 \le (M_B - M_D)^2$ imposed to eliminate the weak annihilation contribution. We consider an additional cut on the hadronic variable $P_+ \le \Delta_P$ (top), or on the hadronic invariant mass $M_X \le M_0$ (bottom). As before, decay rates are given in units of $|V_{ub}|^2 \mathrm{ps}^{-1}$. Predictions are based on the shape-function parameters $m_b = 4.61$ GeV and $\mu_\pi^2 = 0.2$ GeV^2.

Δ_P [GeV]	Mean	Subleading SF	Perturbative	Total
0.70	39.96	± 1.27	$^{+2.16}_{-2.01}$	$^{+2.51}_{-2.38}$
0.65	37.18	± 1.50	$^{+1.99}_{-1.85}$	$^{+2.49}_{-2.38}$
0.60	34.05	± 1.71	$^{+1.82}_{-1.69}$	$^{+2.50}_{-2.41}$
0.55	30.61	± 1.89	$^{+1.63}_{-1.52}$	$^{+2.49}_{-2.42}$
0.50	26.86	± 1.97	$^{+1.44}_{-1.33}$	$^{+2.44}_{-2.38}$
M_0 [GeV]	Mean	Subl. SF	Pert.	Total
M_D	46.75	± 0.65	$^{+2.82}_{-2.50}$	$^{+2.89}_{-2.58}$
1.70	40.70	± 1.12	$^{+2.32}_{-2.11}$	$^{+2.58}_{-2.39}$
1.55	33.69	± 1.56	$^{+1.88}_{-1.73}$	$^{+2.44}_{-2.32}$

The results are summarized in Table VI and can be compared to the previous "pure" P_+ and M_X cuts in Tables III and IV. As an example, let us consider the case $P_+ \le 0.65$ GeV, which is close to the charm threshold. Without the additional q^2 cut we found that the total theoretical uncertainty (including the weak annihilation error) is $^{+7.0}_{-6.8}$%. When cutting in addition on $q^2 \le (M_B - M_D)^2$, the efficiency decreases by about 20% as expected. However, due to the absence of the weak annihilation uncertainty, the overall uncertainty decreases to $^{+6.7}_{-6.4}$%. Therefore both strategies result in comparable relative uncertainties, with a slight favor for imposing the additional cut from the theoretical point of view.

While the small reduction of theoretical errors hardly seems worth the effort of imposing the q^2 cut, performing an analysis of the type outlined here and comparing its results with those obtained without the additional cut may help to corroborate the expectation that the weak annihilation contribution is indeed not much larger than what has been found in [44].

G. Dependence on m_b and shape-function sensitivity

Nonperturbative hadronic physics enters in our approach via the form of the leading and subleading shape functions. The strongest sensitivity by far is to the first moment of the leading shape function, which determines the HQET parameter $\bar{\Lambda}$ and with it the b-quark mass. Given that the value of $m_b \equiv m_b(\mu_*, \mu_*)$ can be determined with good precision from other sources (such as moments of the

leptonic or hadronic invariant mass spectra in $\bar{B} \to X_c l^- \bar{\nu}$ decays), it is instructive to disentangle this dependence from the sensitivity to higher moments or, more generally, to the functional form of the shape functions for fixed m_b.

To explore the dependence on m_b we define the exponent

$$a(m_b) \equiv \frac{d\ln\Gamma_u}{d\ln m_b} = \left(\frac{\triangle\Gamma_u}{\Gamma_u}\right)\Big/\left(\frac{\triangle m_b}{m_b}\right), \tag{68}$$

which means that $\Gamma_u \sim (m_b)^a$. Table VII shows the values of this exponent over a wide range of values of m_b for a variety of experimental cuts. To estimate the sensitivity to the functional form we scan over a large set of models for the subleading shape functions, and we also study the difference between the results obtained using the exponential or the Gaussian ansatz for the leading shape function. The corresponding variations are added in quadrature and given as a relative change in the corresponding partial decay rates (labeled ''Functional Form''). In all cases, $\mu_\pi^2 = 0.2$ GeV^2 is kept fixed. Because we restrict ourselves to only two functional forms for the leading shape function in this study, the resulting sensitivities should be interpreted with caution.

The entries in the table are listed in roughly the order of increasing sensitivity to m_b and to the functional form of the shape functions, with the hadronic invariant mass cut showing the least sensitivity and the lepton energy cut exhibiting the largest one. To some extent this reflects the different efficiencies (or ''inclusiveness'') of the various cuts. It is reassuring that $a \approx 10$ for the pure q^2 cut, in accordance with the findings of [38,39]. Perhaps somewhat surprisingly, for this cut a substantial sensitivity to shape-function effects remains even for fixed m_b and μ_π^2. It is well-known that the partial rate with a cut $q^2 \geq (M_B - M_D)^2$ can be calculated using a local OPE in powers of $\Lambda_{\rm QCD}/m_c$ [38,54], thereby avoiding the notion of shape-function sensitivity. Differences between the functional forms of the shape functions in our approach correspond to effects that are formally of order $1/m_c^3$ and higher. It is not unreasonable that these effects should be of order 3%–5%.

We also checked that for much more relaxed cuts the value of $a(m_b)$ tends to 4.8, as stated in (58). For example, for a cut $P_+ \leq \Delta_P$ we find (with $m_b = 4.61$ GeV and $\mu_\pi^2 = 0.2$ GeV^2):

Δ_P[GeV]	0.6	0.8	1.0	1.2	1.6	2.0	3.0	M_B
a	15.4	9.8	7.0	5.8	5.1	5.0	4.9	4.8

VI. CONCLUSIONS

A high-precision measurement of the parameters of the unitarity triangle is an ongoing quest, which necessitates the close cooperation of theory and experiment. The determination of $|V_{ub}|$ from inclusive $\bar{B} \to X_u l^- \bar{\nu}$ decay requires the measurement of partial decay rates with kinematical cuts that eliminate the large background from $\bar{B} \to X_c l^- \bar{\nu}$ decay, as well as theoretical predictions for such quantities. To this end, it is desirable to have a theoretical description of the triple-differential decay rate, which can be used for predicting arbitrary partial rates obtained after integrating over certain regions of phase space. One problem in providing such a description is that the power-counting rules of the heavy-quark expan-

TABLE VII. Values of the exponent $a(m_b)$ for different kinematical cuts. The parameter $\mu_\pi^2 = 0.2$ GeV^2 is kept fixed. Also quoted is the sensitivity of the partial decay rates to the functional form of the shape functions. See text for explanation.

	m_b [GeV]	4.50	4.55	4.60	4.65	4.70
$M_X \leq M_D$	a	9.5	8.8	8.2	7.7	7.3
	Functional Form	1.4%	1.1%	0.8%	0.5%	0.4%
$M_X \leq 1.7$ GeV	a	12.5	11.5	10.5	9.7	8.9
	Functional Form	2.9%	2.6%	2.2%	1.9%	1.6%
$M_X \leq 1.7$ GeV	a	10.3	9.8	9.3	9.0	8.7
$q^2 \geq 8$ GeV^2	Functional Form	2.0%	1.7%	1.5%	1.4%	1.4%
$q^2 \geq (M_B - M_D)^2$	a	11.4	11.1	10.9	10.8	10.6
	Functional Form	5.0%	4.4%	4.0%	3.6%	3.2%
$P_+ \leq M_D^2/M_B$	a	16.7	15.0	13.6	12.2	11.1
	Functional Form	5.3%	4.8%	4.4%	4.0%	3.6%
$E_l \geq 2.2$ GeV	a	22.6	21.0	19.7	18.5	17.4
	Functional Form	16.2%	13.1%	11.0%	9.3%	7.9%

sion are different in different kinematical domains. In this paper we have overcome this difficulty.

In the shape-function region, our results are in agreement with QCD factorization theorems, and perturbative effects have been separated from nonperturbative shape functions. When the allowed phase space extends over a large domain, our results smoothly reduce to the expressions obtained from the local operator product expansion. We have presented a formalism in which event distributions and partial decay rates are expressed without explicit reference to partonic quantities such as the b-quark mass. The sensitivity to such hadronic parameters enters indirectly, via the moments of shape functions. The most important nonperturbative object, namely the leading-order shape function, can be extracted from the photon spectrum in $\bar{B} \to X_s\gamma$ decay. This is analogous to extractions of parton distribution functions from fits to data on deep inelastic scattering. In this way, the dominant uncertainty from our ignorance about bound-state effects in the B meson is turned into an experimental uncertainty, which will reduce with increasing accuracy of the experimental data on the photon spectrum. Residual hadronic uncertainties are power-suppressed in the heavy-quark expansion.

One goal of this paper was to present a detailed framework in which this program can be carried out. We have given formulas that can be readily used for the construction of an event generator, as well as to estimate the remaining theoretical uncertainties in a robust and automated fashion.

In practice the leading shape function needs to be parameterized. We have suggested three different functional forms, which can be used to fit the data of the $\bar{B} \to X_s\gamma$ photon spectrum. Once the data is accurately described by a choice of the shape functions, this function can be used in the predictions for partial $\bar{B} \to X_u l^- \bar{\nu}$ rates and spectra. Subleading shape functions give rise to theoretical uncertainties starting at the level of $1/m_b$ power corrections. We have estimated these uncertainties using a large set of models, each of which obeys the known tree-level moment relations, but which are very different in their functional form. A second error estimate is determined by the residual renormalization-scale dependence. We also considered uncertainties from weak annihilation effects, which in principle can be avoided by cutting away the region of phase space in which they contribute. We have suggested a cut on high leptonic invariant mass, which accomplishes just that.

The second half of this paper contains detailed numerical predictions for a variety of partial $\bar{B} \to X_u l^- \bar{\nu}$ decay rates with different kinematical cuts, including cuts on the charged-lepton energy (both in the rest frame of the B meson and of the $\Upsilon(4S)$ resonance), on the hadronic quantity $P_+ = E_X - |\vec{P}_X|$, on M_X, on q^2, and on various combinations of these variables. Along with our predictions for the rates we have presented a complete analysis of theoretical uncertainties. Once the data on the $\bar{B} \to X_s\gamma$ photon spectrum are sufficiently precise to accurately determine the leading-order shape function, a determination of $|V_{ub}|$ with theoretical uncertainties at the 5%–10% level now seems feasible.

ACKNOWLEDGMENTS

We are grateful to many of our colleagues in both experiment and theory. We thank Christian Bauer, Ilija Bizjak, Riccardo Faccini, Lawrence Gibbons, Vladimir Golubev, Kay Kinoshita, Robert Kowalewski, Seung Lee, Zoltan Ligeti, Antonio Limosani, Francesca Di Lodovico, Vera Luth, Thomas Meyer, Masahiro Morii, Franz Muheim, and Tadao Nozaki for valuable discussions. We would like to thank the Institute for Advanced Study, Princeton, New Jersey, where part of this work was done, for their hospitality. The work of B. O. L. was supported in part by funds provided by the U.S. Department of Energy (D.O.E.) under cooperative research agreement DE-FC02-94ER40818. The research of M. N. and G. P. was supported by the National Science Foundation under Grant No. PHY-0355005.

APPENDIX A: PERTURBATIVE EXPRESSIONS

1. Anomalous dimensions

Here we list the known perturbative expansions of the β-function and relevant anomalous dimensions. We work in the $\overline{\rm MS}$ scheme and define

$$\begin{aligned}\beta(\alpha_s) &= \frac{d\alpha_s(\mu)}{d\ln\mu} = -2\alpha_s \sum_{n=0}^{\infty} \beta_n \left(\frac{\alpha_s}{4\pi}\right)^{n+1},\\ \Gamma_{\rm cusp}(\alpha_s) &= \sum_{n=0}^{\infty} \Gamma_n \left(\frac{\alpha_s}{4\pi}\right)^{n+1},\\ \gamma'(\alpha_s) &= \sum_{n=0}^{\infty} \gamma'_n \left(\frac{\alpha_s}{4\pi}\right)^{n+1},\end{aligned} \tag{A1}$$

as the expansion coefficients for the β-function, the leading-order SCET current anomalous dimension, and the cusp anomalous dimension. To three-loop order, the β-function reads [57]

$$\begin{aligned}\beta_0 &= \frac{11}{3}C_A - \frac{2}{3}n_f,\\ \beta_1 &= \frac{34}{3}C_A^2 - \frac{10}{3}C_A n_f - 2C_F n_f,\\ \beta_2 &= \frac{2857}{54}C_A^3 + \left(C_F^2 - \frac{205}{18}C_F C_A - \frac{1415}{54}C_A^2\right)n_f\\ &\quad + \left(\frac{11}{9}C_F + \frac{79}{54}C_A\right)n_f^2,\end{aligned} \tag{A2}$$

where $n_f = 4$ is the number of light flavors, $C_A = 3$ and $C_F = 4/3$. The three-loop expression for the cusp anomalous dimension has recently been obtained in [58]. The coefficients read

$$\begin{aligned}
\Gamma_0 &= 4C_F,\\
\Gamma_1 &= 8C_F\biggl[\Bigl(\frac{67}{18}-\frac{\pi^2}{6}\Bigr)C_A-\frac{5}{9}n_f\biggr],\\
\Gamma_2 &= 16C_F\biggl[\Bigl(\frac{245}{24}-\frac{67\pi^2}{54}+\frac{11\pi^4}{180}+\frac{11}{6}\zeta_3\Bigr)C_A^2\\
&\quad+\Bigl(-\frac{209}{108}+\frac{5\pi^2}{27}-\frac{7}{3}\zeta_3\Bigr)C_An_f\\
&\quad+\Bigl(-\frac{55}{24}+2\zeta_3\Bigr)C_Fn_f-\frac{1}{27}n_f^2\biggr].
\end{aligned}\tag{A3}$$

The SCET anomalous dimension γ is explicitly known only to one-loop order. However, the two-loop coefficient can be extracted by noting that γ is related to the axial-gauge anomalous dimension in deep inelastic scattering [11]. The result is

$$\begin{aligned}
\gamma_0' &= -5C_F,\\
\gamma_1' &= -8C_F\biggl[\Bigl(\frac{3}{16}-\frac{\pi^2}{4}+3\zeta_3\Bigr)C_F\\
&\quad+\Bigl(\frac{1549}{432}+\frac{7\pi^2}{48}-\frac{11}{4}\zeta_3\Bigr)C_A-\Bigl(\frac{125}{216}+\frac{\pi^2}{24}\Bigr)n_f\biggr].
\end{aligned}\tag{A4}$$

2. Evolution factor

The exact expression for the evolution factor reads

$$\begin{aligned}
\ln U(\mu_h,\mu_i) &= 2S_\Gamma(\mu_h,\mu_i)-2a_\Gamma(\mu_h,\mu_i)\ln\frac{m_b}{\mu_h}\\
&\quad-2a_{\gamma'}(\mu_h,\mu_i),
\end{aligned}\tag{A5}$$

where the functions of the right-hand side are solutions to the renormalization group equations

$$\begin{aligned}
\frac{d}{d\ln\mu}S_\Gamma(\nu,\mu) &= -\Gamma_{\rm cusp}(\alpha_s(\mu))\ln\frac{\mu}{\nu},\\
\frac{d}{d\ln\mu}a_\Gamma(\nu,\mu) &= -\Gamma_{\rm cusp}(\alpha_s(\mu)),\\
\frac{d}{d\ln\mu}a_{\gamma'}(\nu,\mu) &= -\gamma'(\alpha_s(\mu)),
\end{aligned}\tag{A6}$$

with boundary conditions $S(\nu,\mu)=0$ etc. at $\mu=\nu$. These equations can be integrated using that $d/d\ln\mu = \beta(\alpha_s)d/d\alpha_s$. The solutions are

$$\begin{aligned}
S_\Gamma(\nu,\mu) &= -\int_{\alpha_s(\nu)}^{\alpha_s(\mu)}d\alpha\,\frac{\Gamma_{\rm cusp}(\alpha)}{\beta(\alpha)}\int_{\alpha_s(\nu)}^{\alpha}\frac{d\alpha'}{\beta(\alpha')},\\
a_\Gamma(\nu,\mu) &= -\int_{\alpha_s(\nu)}^{\alpha_s(\mu)}d\alpha\,\frac{\Gamma_{\rm cusp}(\alpha)}{\beta(\alpha)},
\end{aligned}\tag{A7}$$

and similarly for $a_{\gamma'}$.

Next, we give explicit results for the Sudakov exponent S_Γ and the functions a_Γ and a_γ in (A5) at next-to-leading order in renormalization-group improved perturbation theory. We obtain

$$\begin{aligned}
a_\Gamma(\nu,\mu) &= \frac{\Gamma_0}{2\beta_0}\biggl[\ln\frac{\alpha_s(\mu)}{\alpha_s(\nu)}+\Bigl(\frac{\Gamma_1}{\Gamma_0}-\frac{\beta_1}{\beta_0}\Bigr)\frac{\alpha_s(\mu)-\alpha_s(\nu)}{4\pi}\\
&\quad+\ldots\biggr],
\end{aligned}\tag{A8}$$

and similarly for a_γ. The next-to-leading order expressions for the Sudakov exponent S_Γ contains the three-loop coefficients β_2 and Γ_2. With $r=\alpha_s(\mu)/\alpha_s(\nu)$, it reads

$$\begin{aligned}
S_\Gamma(\nu,\mu) &= \frac{\Gamma_0}{4\beta_0^2}\biggl\{\frac{4\pi}{\alpha_s(\nu)}\Bigl(1-\frac{1}{r}-\ln r\Bigr)+\Bigl(\frac{\Gamma_1}{\Gamma_0}-\frac{\beta_1}{\beta_0}\Bigr)\\
&\quad\times(1-r+\ln r)+\frac{\beta_1}{2\beta_0}\ln^2 r\\
&\quad+\frac{\alpha_s(\nu)}{4\pi}\biggl[\Bigl(\frac{\beta_1\Gamma_1}{\beta_0\Gamma_0}-\frac{\beta_2}{\beta_0}\Bigr)(1-r+r\ln r)\\
&\quad+\Bigl(\frac{\beta_1^2}{\beta_0^2}-\frac{\beta_2}{\beta_0}\Bigr)(1-r)\ln r\\
&\quad-\Bigl(\frac{\beta_1^2}{\beta_0^2}-\frac{\beta_2}{\beta_0}-\frac{\beta_1\Gamma_1}{\beta_0\Gamma_0}+\frac{\Gamma_2}{\Gamma_0}\Bigr)\frac{(1-r)^2}{2}\biggr]+\ldots\biggr\}.
\end{aligned}\tag{A9}$$

The next-to-leading-logarithmic evolution factor $U(\mu_h,\mu_i)$ can be obtained by combining the above expressions according to (A5) and expanding out terms of order α_s.

APPENDIX B: PARTIALLY INTEGRATED DECAY RATES

With the exception of the combined cut on the lepton energy E_l and the hadronic quantity $s_H^{\rm max}$ studied in Sec. V E, all other partial rates investigated in our analysis can be derived by first integrating the triple-differential decay rate (23) over the lepton energy $E_l\ge E_0$ and $P_-\le P_-^{\rm max}$ analytically, where the quantity $P_-^{\rm max}$ (and in principle even E_0) may depend on the value of P_+. The remaining integration over P_+ is then performed numerically. In such a situation, we need to evaluate the partially integrated decay rate

$$\frac{d\Gamma_u}{dP_+}=\int_{P_+}^{P_-^{\rm max}}dP_-\int_{P_+}^{\min(P_-,M_B-2E_0)}dP_l\,\frac{d^3\Gamma_u}{dP_l dP_- dP_+}.\tag{B1}$$

Changing variables from P_- to y defined in (25), the constraint $P_-\le P_-^{\rm max}$ translates into the integration domain $0\le y\le y_{\rm max}$, where in analogy to (25) we define

$$\begin{aligned}
y_{\rm max} &= \frac{P_-^{\rm max}-P_+}{M_B-P_+},\\
y_0 &= \frac{P_l^{\rm max}-P_+}{M_B-P_+}=1-\frac{2E_0}{M_B-P_+}.
\end{aligned}\tag{B2}$$

From the phase-space relation (2) it follows that a cut on the lepton energy has no effect if $y_0\ge y_{\rm max}$. The result of

performing the integrations in (B1) can be written as

$$\frac{d\Gamma_u(y_{\max}, y_0)}{dP_+} = \begin{cases} \Gamma_u^A(y_{\max}); & y_{\max} \le y_0, \\ \Gamma_u^A(y_0) + \Gamma_u^B; & y_{\max} > y_0, \end{cases} \tag{B3}$$

where

$$\begin{aligned} \Gamma_u^A(y_i) &= \frac{G_F^2|V_{ub}|^2}{96\pi^3}(M_B - P_+)^5 U(\mu_h, \mu_i) \\ &\quad \times \int_0^{y_i} dy\, y^{2-2a_\Gamma}[(3-2y)\mathcal{F}_1 + 6(1-y)\mathcal{F}_2 \\ &\quad + y\mathcal{F}_3], \\ \Gamma_u^B &= \frac{G_F^2|V_{ub}|^2}{96\pi^3}(M_B - P_+)^5 U(\mu_h, \mu_i) \\ &\quad \times \int_{y_0}^{y_{\max}} dy\, y^{-2a_\Gamma} y_0[(6y(1+y_0) - 6y^2 \\ &\quad - y_0(3+2y_0))\mathcal{F}_1 + 6y(1-y)\mathcal{F}_2 \\ &\quad + y_0(3y - 2y_0)\mathcal{F}_3]. \end{aligned} \tag{B4}$$

When the kinematical power corrections in (30) are expanded as in (32) and (33), the resulting integrals over y can be expressed in terms of the master functions $I_n(b, z)$ given in eq. (86) of [9]. The resulting expressions are used to obtain the numbers in the various tables in Sec. V.

We now list the values of y_0 and $y_{\max}$ for the different cuts studied in Sec. V. Whenever a cut $E_l \ge E_0$ on the charged-lepton energy is applied, we have

$$y_0 = 1 - \frac{2E_0}{M_B - P_+}. \tag{B5}$$

For an additional cut $P_+ \le \Delta_P$, we have $y_{\max} = 1$ and $0 \le P_+ \le \min(\Delta_P, M_B - 2E_0)$. For a cut on hadronic invariant mass, $M_X \le M_0$, we have

$$y_{\max} = \frac{\min(M_B, M_0^2/P_+) - P_+}{M_B - P_+} \tag{B6}$$

and $0 \le P_+ \le \min(M_0, M_B - 2E_0)$. For a cut on leptonic invariant mass, $q^2 \ge q_0^2$, we have

$$y_{\max} = 1 - \frac{q_0^2}{(M_B - P_+)^2} \tag{B7}$$

and $0 \le P_+ \le \min(M_B - q_0, M_B - 2E_0)$. Finally, for the combined M_X–q^2 cut we take the minimum of the previous two $y_{\max}$ values.

[1] B. Aubert *et al.* (*BABAR* Collaboration), Phys. Rev. Lett. **94**, 161 803 (2005).
[2] K. Abe *et al.* (Belle Collaboration), Phys. Rev. D **71**, 072 003 (2005); **71**, 079 903 (2005).
[3] M. Neubert, Phys. Rev. D **49**, 3392 (1994).
[4] M. Neubert, Phys. Rev. D **49**, 4623 (1994).
[5] I. I. Y. Bigi, M. A. Shifman, N. G. Uraltsev, and A. I. Vainshtein, Int. J. Mod. Phys. A **9**, 2467 (1994).
[6] G. P. Korchemsky and G. Sterman, Phys. Lett. B **340**, 96 (1994).
[7] R. Akhoury and I. Z. Rothstein, Phys. Rev. D **54**, 2349 (1996).
[8] C. W. Bauer and A. V. Manohar, Phys. Rev. D **70**, 034 024 (2004).
[9] S. W. Bosch, B. O. Lange, M. Neubert, and G. Paz, Nucl. Phys. **B699**, 335 (2004).
[10] E. Gardi, J. High Energy Phys. 04 (2004) 049.
[11] M. Neubert, Eur. Phys. J. C **40**, 165 (2005).
[12] B. Blok, L. Koyrakh, M. A. Shifman, and A. I. Vainshtein, Phys. Rev. D **49**, 3356 (1994); **50**, 3572(E) (1994).
[13] A. V. Manohar and M. B. Wise, Phys. Rev. D **49**, 1310 (1994).
[14] S. W. Bosch, B. O. Lange, M. Neubert, and G. Paz, Phys. Rev. Lett. **93**, 221 801 (2004).
[15] F. J. Tackmann, Phys. Rev. D **72**, 034 036 (2005).
[16] S. W. Bosch, M. Neubert, and G. Paz, J. High Energy Phys. 11 (2004) 073.
[17] A. K. Leibovich, I. Low, and I. Z. Rothstein, Phys. Rev. D **61**, 053 006 (2000).
[18] A. K. Leibovich, I. Low, and I. Z. Rothstein, Phys. Lett. B **486**, 86 (2000).
[19] M. Neubert, Phys. Lett. B **513**, 88 (2001).
[20] A. L. Kagan and M. Neubert, Eur. Phys. J. C **7**, 5 (1999).
[21] K. G. Chetyrkin, M. Misiak, and M. Munz, Phys. Lett. B **400**, 206 (1997)**425**, 414(E) (1998).
[22] F. De Fazio and M. Neubert, J. High Energy Phys. 06 (1999) 017.
[23] C. Greub, T. Hurth, and D. Wyler, Phys. Rev. D **54**, 3350 (1996).
[24] A. Ali and C. Greub, Phys. Lett. B **361**, 146 (1995).
[25] R. J. Hill, T. Becher, S. J. Lee, and M. Neubert, J. High Energy Phys. 07 (2004) 081.
[26] T. Becher, R. J. Hill, B. O. Lange, and M. Neubert, Phys. Rev. D **69**, 034 013 (2004).
[27] C. W. Bauer, M. E. Luke, and T. Mannel, Phys. Rev. D **68**, 094 001 (2003).
[28] C. W. Bauer, M. Luke, and T. Mannel, Phys. Lett. B **543**, 261 (2002).
[29] A. K. Leibovich, Z. Ligeti, and M. B. Wise, Phys. Lett. B **539**, 242 (2002).
[30] M. Neubert, Phys. Lett. B **543**, 269 (2002).
[31] K. S. M. Lee and I. W. Stewart, Nucl. Phys. **B721**, 325 (2005).
[32] M. Beneke, F. Campanario, T. Mannel, and B. D. Pecjak, J. High Energy Phys. 06 (2005) 071.
[33] A. F. Falk and M. Neubert, Phys. Rev. D **47**, 2965 (1993).
[34] M. Neubert, Phys. Rep. **245**, 259 (1994).
[35] G. Martinelli, M. Neubert, and C. T. Sachrajda, Nucl. Phys. **B461**, 238 (1996).
[36] M. Neubert, Phys. Lett. B **393**, 110 (1997).

[37] A. F. Falk, M. E. Luke, and M. J. Savage, Phys. Rev. D **49**, 3367 (1994).
[38] M. Neubert, J. High Energy Phys. 07 (2000) 022.
[39] M. Neubert and T. Becher, Phys. Lett. B **535**, 127 (2002).
[40] N. Uraltsev, Int. J. Mod. Phys. A **14**, 4641 (1999).
[41] I. I. Y. Bigi and N. G. Uraltsev, Nucl. Phys. **B423**, 33 (1994).
[42] M. Neubert and C. T. Sachrajda, Nucl. Phys. **B483**, 339 (1997).
[43] M. B. Voloshin, Phys. Lett. B **515**, 74 (2001).
[44] T. O. Meyer, Ph.D. thesis, Cornell University, 2005.
[45] M. Neubert, hep-ph/0411027
[46] B. Aubert *et al.* (*BABAR* Collaboration), Phys. Rev. Lett. **93**, 011 803 (2004).
[47] M. Beneke, Phys. Lett. B **434**, 115 (1998).
[48] A. H. Hoang, Z. Ligeti, and A. V. Manohar, Phys. Rev. D **59**, 074 017 (1999).
[49] I. I. Y. Bigi, M. A. Shifman, N. Uraltsev, and A. I. Vainshtein, Phys. Rev. D **56**, 4017 (1997).
[50] M. Neubert, Phys. Lett. B **612**, 13 (2005).
[51] T. van Ritbergen, Phys. Lett. B **454**, 353 (1999).
[52] A. F. Falk, Z. Ligeti, and M. B. Wise, Phys. Lett. B **406**, 225 (1997).
[53] I. I. Y. Bigi, R. D. Dikeman, and N. Uraltsev, Eur. Phys. J. C **4**, 453 (1998).
[54] C. W. Bauer, Z. Ligeti, and M. E. Luke, Phys. Lett. B **479**, 395 (2000).
[55] C. W. Bauer, Z. Ligeti, and M. E. Luke, Phys. Rev. D **64**, 113 004 (2001).
[56] B. Aubert *et al.* (*BABAR* Collaboration), hep-ex/0408045.
[57] O. V. Tarasov, A. A. Vladimirov, and A. Y. Zharkov, Phys. Lett. B **93**, 429 (1980).
[58] S. Moch, J. A. M. Vermaseren, and A. Vogt, Nucl. Phys. **B688**, 101 (2004).